

Appendix A

Groundwater Risk Pathway Model Development, Calibration and Predictive Results

**Peter Martian
Chinnathambi Esakkiperumal
Annette L. Schafer**

TABLE OF CONTENTS

A-1 INTRODUCTION	A-1-1
A-1.1 Report Organization	A-1-1
A-2 MODELING PURPOSE AND MOTIVATION.....	A-1-1
A-2.1 Purpose	A-1-1
A-2.2 Motivation	A-1-1
A-3 SUMMARY OF VADOSE ZONE DATA	A-3-1
A-3.1 Vadose Zone Geology and Lithology.....	A-3-1
A-3.2 Vadose Zone Hydrological Data	A-3-2
A-3.2.1 Surficial Alluvium.....	A-3-2
A-3.2.2 Vadose Zone Basalt	A-3-3
A-3.2.3 Interbeds	A-3-4
A-3.3 Vadose Zone Infiltration from Precipitation.....	A-3-6
A-3.4 Perched Water Depth and Soil Moisture/Tension	A-3-8
A-3.5 Vadose Zone Water Chemistry	A-3-22
A-3.6 Vadose Zone Water Sources	A-3-23
A-3.7 Vadose Zone Solute Sorption Data.....	A-3-27
A-4 AQUIFER DATA SUMMARY	A-4-1
A-4.1 Aquifer Geology/Lithology.....	A-4-1
A-4.2 Aquifer Hydrological Data.....	A-4-3
A-4.2.1 Aquifer Hydraulic Conductivity	A-4-3
A-4.3 Aquifer Water Chemistry	A-4-6
A-5 VADOSE ZONE AND AQUIFER CONCEPTUAL MODELS	A-5-1
A-5.1 Vadose Zone Model and Parameterization.....	A-5-1
A-5.1.1 Representation of Lithology.....	A-5-2
A-5.1.2 Vadose Zone Simulation Domain and Discretization	A-5-5
A-5.1.3 Incorporating Infiltration.....	A-5-8
A-5.1.4 Contaminant Source Terms for Model Calibration.....	A-5-13
A-5.1.5 Vadose Zone Initial Conditions	A-5-14
A-5.2 Aquifer Model and Parameterization	A-5-17
A-5.2.1 Representation of Lithology and Hydrology.....	A-5-18
A-5.2.2 Aquifer Simulation Domain and Discretization.....	A-5-21
A-5.2.3 Aquifer Boundary Conditions and Water Sources	A-5-23
A-5.2.4 Aquifer Initial Conditions	A-5-24
A-5.3 Simulation Code	A-5-25
A-6 SIMULATION CODE.....	A-6-1
A-6.1 Modifications to Version 12.7 Resulting in Version 12.7ms.....	A-6-4
A-6.2 Quality Assurance	A-6-4
A-7 VADOSE ZONE MODEL CALIBRATION	A-7-1
A-7.1 Specific Data Used In Vadose Zone Model Calibration	A-7-3

A-7.1.1	Water Level Data.....	A-7-3
A-7.1.2	Water Chemistry Data	A-7-4
A-7.2	Vadose Zone Flow Calibration Results	A-7-4
A-7.2.1	Northern Upper Shallow Perched Water	A-7-12
A-7.2.2	Northern Lower Shallow Perched Water	A-7-15
A-7.2.3	Northern Deep Perched Water.....	A-7-16
A-7.2.4	Southern Shallow Perched Water	A-7-18
A-7.2.5	Southern Deep Perched Water.....	A-7-21
A-7.3	Vadose Zone Transport Calibration.....	A-7-23
A-7.3.1	Tc-99.....	A-7-24
A-7.3.2	Tritium.....	A-7-32
A-7.3.3	I-129	A-7-40
A-7.3.4	Nitrate.....	A-7-48
A-7.3.5	Transport Calibration Conclusions.....	A-7-55
A-7.4	Summary of Vadose Zone Model Assumptions	A-7-56
A-8	AQUIFER MODEL CALIBRATION	A-8-1
A-8.1	Specific Calibration Data For the Aquifer Model.....	A-8-1
A-8.1.1	Calibration Data for the Flow Model	A-8-1
A-8.1.2	Calibration Data for the Transport Model	A-8-2
A-8.2	Aquifer Flow Calibration	A-8-7
A-8.3	Aquifer Transport Model Calibration.....	A-8-9
A-8.3.1	Tritium in the Aquifer	A-8-12
A-8.3.2	Technetium-99 in the Aquifer	A-8-20
A-8.3.3	Iodine-129 in the Aquifer.....	A-8-28
A-8.3.4	Nitrate in the Aquifer	A-8-36
A-8.3.5	Aquifer Flow Model Calibration Conclusions	A-8-40
A-8.3.6	Aquifer Transport Model Calibration Conclusions.....	A-8-40
A-8.4	Summary of Aquifer Model Assumptions	A-8-40
A-9	GROUNDWATER PATHWAY RISK PREDICTION	A-9-1
A-9.1	Screening Analysis	A-9-1
A-9.1.1	Results of GWSCREEN Analysis	A-9-6
A-9.2	Contaminants of Potential Concern Source Terms	A-9-10
A-9.2.1	Release Estimates for OU 3-14 Sites	A-9-11
A-9.2.2	Remaining OU 3-13 Sites	A-9-13
A-9.2.3	Service Waste	A-9-14
A-9.3	Groundwater Simulation Results	A-9-15
A-9.3.1	H-3.....	A-9-18
A-9.3.2	I-129	A-9-23
A-9.3.3	Np-237.....	A-9-29
A-9.3.4	Pu-239	A-9-34
A-9.3.5	Pu-240	A-9-38
A-9.3.6	Tc-99.....	A-9-42
A-9.3.7	U-234.....	A-9-48
A-9.3.8	Mercury	A-9-50

A-9.3.9 Nitrate	A-9-55
A-9.3.10 Groundwater Pathway Simulation Results Summary	A-9-60
A-10ASSESSMENT OF MODEL LIMITATIONS	A-10-1
A-10.1 Model Sensitivity Analysis	A-10-1
A-10.1.1 Interbed Thickness and Permeability	A-10-2
A-10.1.2 Recharge Rate	A-10-17
A-10.1.3 Tc-99 Preferential Flow Between the 380-ft Interbed and the ICPP-MON-A-230 Well	A-10-36
A-10.1.4 Tc-99 Service Waste Source Inventory	A-10-39
A-10.1.5 Model Horizontal Grid Size	A-10-46
A-10.1.6 Sensitivity Analysis Summary	A-10-53
A-10.2 Model Uncertainty Analysis	A-10-56
A-10.2.1 Conceptual Model Uncertainty	A-10-56
A-10.2.2 Parametric Uncertainty	A-10-57
A-10.2.3 Model Uncertainty Summary	A-10-62
A-11REFERENCES	A-11-1

LIST OF FIGURES

A-1 INTRODUCTION

A-1-1	Map showing the location of the INL Site, INTEC, and the tank farm.	A-1-3
-------	--	-------

A-3 SUMMARY OF VADOSE ZONE DATA

A-3-1	Aquifer and perched water well locations.	A-3-10
A-3-2	Alluvium perched water well locations and hydrographs.	A-3-11
A-3-3	Northern upper shallow perched water well locations and hydrographs.	A-3-12
A-3-4	Northern lower shallow perched water well locations and hydrographs.	A-3-13
A-3-5	Northern deep perched water well locations and hydrographs.	A-3-14
A-3-6	Southern upper shallow perched water well locations and hydrographs.	A-3-15
A-3-7	Southern lower shallow perched water well locations and hydrographs.	A-3-16
A-3-8	Southern deep perched water well locations and hydrographs.	A-3-17
A-3-9	Mean streamflow and Big Lost River losses.	A-3-25

A-4 AQUIFER DATA SUMMARY

A-4-1	Deep INL Site wells used to define the aquifer thickness.	A-4-2
-------	--	-------

A-5 VADOSE ZONE AND AQUIFER CONCEPTUAL MODELS

A-5-1	Vadose zone structure.	A-5-5
A-5-2	Tank farm submodel vadose horizontal discretization.	A-5-6
A-5-3	Large-scale vadose zone model horizontal discretization.	A-5-7
A-5-4	Vadose zone model vertical discretization with 35x vertical exaggeration.	A-5-8
A-5-5	Areal distribution of the pre-remedial action rates.	A-5-10
A-5-6	Areal distribution of the post-remedial action water balance.	A-5-12
A-5-7	Tank farm submodel horizontal discretization.	A-5-16
A-5-8	Large-scale vadose zone model horizontal discretization.	A-5-17
A-5-9	Aquifer model thickness.	A-5-19
A-5-10	Initial H basalt hydraulic conductivity field.	A-5-21
A-5-11	Aquifer model domain and horizontal discretization.	A-5-22
A-5-12	Aquifer model vertical discretization with 30x vertical exaggeration.	A-5-23

A-7 VADOSE ZONE MODEL CALIBRATION

A-7-1	Horizontal extent of simulated perched water.	A-7-7
A-7-2	Simulated saturation versus depth for northern perched water well locations	A-7-8
A-7-3	Simulated saturation versus depth for northern perched water well locations	A-7-9
A-7-4	Simulated saturation versus depth for southern perched water well locations.	A-7-10
A-7-5	Simulated saturation versus depth for southern perched water well locations.	A-7-11
A-7-6	Simulated saturation versus depth for southern perched water well locations.	A-7-12
A-7-7	Time series water elevation plots for the northern upper shallow perched water	A-7-14
A-7-8	Time series water elevation plots for the northern upper shallow perched water, continued.	A-7-15
A-7-9	Time series water elevation plots for the northern lower shallow perched water	A-7-16
A-7-10	Time series water elevation plots for the northern deep perched water	A-7-17

A-7-11	Time series water elevation plots for the southern shallow perched water	A-7-19
A-7-12	Time series water elevation plots for the southern shallow perched water, continued	A-7-20
A-7-13	Time series water elevation plots for the southern deep perched water	A-7-22
A-7-14	Time series water elevation plots for the southern deep perched water, continued	A-7-23
A-7-15	Total flux of Tc-99 entering the aquifer.....	A-7-25
A-7-16	Horizontal extent of simulated Tc-99 at different depth intervals in the vadose zone in 2004	A-7-26
A-7-17	Tc-99 concentrations in the northern upper shallow perched water	A-7-28
A-7-18	Tc-99 concentration history in the northern lower shallow perched water	A-7-29
A-7-19	Tc-99 concentration history in the northern deep perched water	A-7-30
A-7-20	Tc-99 concentration history in the southern shallow perched water	A-7-31
A-7-21	Tc-99 concentration history in the southern deep perched water	A-7-32
A-7-22	Total flux of H-3 entering the aquifer.....	A-7-33
A-7-23	Horizontal extent of simulated tritium at different depth intervals in 2004.....	A-7-34
A-7-24	Tritium concentration history in the northern upper shallow perched water	A-7-36
A-7-25	Tritium concentration history in the northern upper shallow perched water	A-7-37
A-7-26	Tritium concentration history in the northern deep perched water	A-7-38
A-7-27	Tritium concentration history in the southern shallow perched water	A-7-39
A-7-28	Tritium concentration history in the southern deep perched water	A-7-40
A-7-29	Total flux of I-129 entering the aquifer.	A-7-41
A-7-30	Horizontal extent of simulated I-129 at different depth intervals in 2004.	A-7-42
A-7-31	I-129 concentration history in the northern upper shallow perched water	A-7-44
A-7-32	I-129 concentration history in the northern lower shallow perched water	A-7-45
A-7-33	I-129 concentration history in the northern deep perched water	A-7-46
A-7-34	I-129 concentration history in the southern shallow perched water	A-7-47
A-7-35	I-129 concentration history in the southern deep perched water	A-7-48
A-7-36	Total flux of nitrate entering the aquifer.....	A-7-49
A-7-37	Horizontal extent of simulated nitrate at different depth intervals in 2004.	A-7-50
A-7-38	Nitrate concentration history in the northern upper shallow perched water	A-7-52
A-7-39	Nitrate concentration history in the northern lower shallow perched water	A-7-53
A-7-40	Nitrate concentration history in the northern deep perched water	A-7-53
A-7-41	Nitrate concentration history in the southern shallow perched water	A-7-54
A-7-42	Nitrate concentration history in the southern deep perched water	A-7-55

A-8 AQUIFER MODEL CALIBRATION

A-8-1	WAG-10 regional water levels based on summer 2004 field measurements.....	A-8-2
A-8-2	Reported and simulated tritium disposal in CPP-03.	A-8-4
A-8-3	Reported and simulated technetium-99 disposal in CPP-03.	A-8-5
A-8-4	Reported and simulated strontium-90 disposal in CPP-03.	A-8-5
A-8-5	Reported and simulated iodine-129 disposal in CPP-03.....	A-8-6
A-8-6	Reported and simulated nitrate disposal in CPP-03.....	A-8-6
A-8-7	Predicted hydraulic head and summer 2004 observations	A-8-8
A-8-8	Predicted hydraulic head with summer 2004 observations near INTEC	A-8-9

A-8-9	Aquifer wells located near INTEC.....	A-8-11
A-8-10	Aquifer wells located far from INTEC.	A-8-12
A-8-11	Maximum simulated tritium concentrations in base grid.....	A-8-13
A-8-12	Simulated and measured tritium vs. depth at vertical boreholes in 2003.....	A-8-14
A-8-13	Simulated and observed tritium concentration histories.	A-8-15
A-8-14	Simulated and observed tritium concentration histories	A-8-16
A-8-15	Simulated and observed tritium concentration histories.	A-8-17
A-8-16	Simulated and observed tritium concentration histories.	A-8-18
A-8-17	Simulated and observed tritium concentration histories.	A-8-19
A-8-18	Simulated maximum Tc-99 concentrations near INTEC	A-8-21
A-8-19	Simulated maximum Tc-99 concentrations in base grid in 1999.....	A-8-22
A-8-20	Simulated Tc-99 peak aquifer concentrations averaged over a 15-m well screen.	A-8-22
A-8-21	Simulated and measured Tc-99 vs. depth at vertical boreholes in 2003	A-8-23
A-8-22	Simulated and observed Tc-99 concentration histories.....	A-8-24
A-8-23	Simulated and observed Tc-99 concentration histories.....	A-8-25
A-8-24	Simulated and observed Tc-99 concentration histories.....	A-8-26
A-8-25	Simulated and observed Tc-99 concentration histories.....	A-8-27
A-8-26	Maximum simulated I-129 concentrations in base grid in 2004.....	A-8-29
A-8-27	Simulated and observed I-129 concentrations vs. depth at vertical boreholes in 2003	A-8-30
A-8-28	Simulated and observed I-129 concentration histories.	A-8-31
A-8-29	Simulated and observed I-129 concentration histories.	A-8-32
A-8-30	Simulated and observed I-129 concentration histories.	A-8-33
A-8-31	Simulated and observed I-129 concentration histories.	A-8-34
A-8-32	Simulated and observed I-129 concentration histories.	A-8-35
A-8-33	Maximum simulated nitrate concentration in base grid in 2004.....	A-8-36
A-8-34	Simulated and observed nitrate concentration histories.....	A-8-37
A-8-35	Simulated and observed nitrate concentration histories.....	A-8-38
A-8-36	Simulated and observed nitrate concentration histories.....	A-8-39

A-9 GROUNDWATER PATHWAY RISK PREDICTION

A-9-1	Conceptual model for GWSCREEN.....	A-9-3
A-9-2	H-3 horizontal vadose zone concentrations	A-9-19
A-9-3	H-3 vertical vadose zone concentrations.....	A-9-20
A-9-4	H-3 peak vadose zone concentrations	A-9-20
A-9-5	H-3 peak activity flux into the aquifer.	A-9-21
A-9-6	H-3 horizontal aquifer concentrations.....	A-9-22
A-9-7	H-3 peak aquifer concentrations.	A-9-23
A-9-8	I-129 horizontal vadose zone concentrations.....	A-9-25
A-9-9	I-129 vertical vadose zone concentrations.	A-9-26
A-9-10	I-129 peak vadose zone concentrations	A-9-26
A-9-11	I-129 peak activity flux into the aquifer.	A-9-27
A-9-12	I-129 horizontal aquifer concentrations.	A-9-28

A-9-13	I-129 peak aquifer concentrations.	A-9-29
A-9-14	Np-237 horizontal vadose zone concentrations.	A-9-30
A-9-15	Np-237 vertical vadose zone concentrations.	A-9-31
A-9-16	Np-237 peak vadose zone concentrations	A-9-31
A-9-17	Np-237 activity flux into the aquifer.	A-9-32
A-9-18	Np-237 horizontal aquifer concentrations.	A-9-33
A-9-19	Np-237 peak aquifer concentrations.	A-9-34
A-9-20	Pu-239 horizontal vadose zone concentrations.	A-9-36
A-9-21	Pu-239 vertical vadose zone concentrations.	A-9-37
A-9-22	Pu-239 peak vadose zone concentrations	A-9-37
A-9-23	Pu-239 activity flux into the aquifer.	A-9-38
A-9-24	Pu-239 peak aquifer concentrations.	A-9-38
A-9-25	Pu-240 horizontal vadose zone concentrations.	A-9-40
A-9-26	Pu-240 vertical vadose zone concentrations.	A-9-41
A-9-27	Pu-240 peak vadose zone concentrations	A-9-41
A-9-28	Pu-240 activity flux into the aquifer.	A-9-42
A-9-29	Pu-240 peak aquifer concentrations.	A-9-42
A-9-30	Tc-99 horizontal vadose zone concentrations.	A-9-44
A-9-31	Tc-99 vertical vadose zone concentrations.	A-9-45
A-9-32	Tc-99 peak vadose zone concentrations	A-9-45
A-9-33	Tc-99 activity flux into the aquifer.	A-9-46
A-9-34	Tc-99 horizontal aquifer concentrations.	A-9-47
A-9-35	Tc-99 peak aquifer concentrations.	A-9-48
A-9-36	U-234 peak vadose zone concentrations	A-9-49
A-9-37	U-234 mass flux into the aquifer.	A-9-49
A-9-38	U-234 peak aquifer concentrations.	A-9-49
A-9-39	Mercury horizontal vadose zone concentrations.	A-9-51
A-9-40	Mercury vertical vadose zone concentrations.	A-9-52
A-9-41	Mercury peak vadose zone concentrations	A-9-52
A-9-42	Mercury mass flux into the aquifer.	A-9-53
A-9-43	Mercury horizontal aquifer concentrations.	A-9-54
A-9-44	Mercury peak aquifer concentrations.	A-9-55
A-9-45	Nitrate horizontal vadose zone concentrations.	A-9-56
A-9-46	Nitrate vertical vadose zone concentrations.	A-9-57
A-9-47	Nitrate peak vadose zone concentrations	A-9-57
A-9-48	Nitrate aquifer mass concentration history.	A-9-58
A-9-49	Nitrate horizontal aquifer concentrations.	A-9-59
A-9-50	Nitrate peak aquifer concentrations.	A-9-60

A-10 ASSESSMENT OF MODEL LIMITATIONS

A-10-1	Highest interbed conductance simulation horizontal extent of simulated perched water.	A-10-3
A-10-2	Lowest interbed conductance simulation horizontal extent of simulated perched water.	A-10-4

A-10-3	Tc-99 horizontal vadose zone concentrations for the highest conductance case .	A-10-6
A-10-4	Tc-99 vertical vadose zone concentrations for the highest conductance case	A-10-7
A-10-5	Tc-99 peak vadose zone concentrations for the highest conductance case.	A-10-7
A-10-6	Tc-99 flux into the aquifer for the highest conductance case.	A-10-8
A-10-7	Tc-99 concentration in perched water wells for the highest conductance case	A-10-9
A-10-8	Tc-99 aquifer concentrations for the highest conductance case	A-10-10
A-10-9	Tc-99 peak aquifer concentrations for the highest conductance case.	A-10-11
A-10-10	Tc-99 horizontal vadose zone concentrations for the lowest conductance case .	A-10-12
A-10-11	Tc-99 vertical vadose zone concentrations for the lowest conductance case	A-10-13
A-10-12	Tc-99 peak vadose zone concentrations for the lowest conductance case.	A-10-13
A-10-13	Tc-99 flux into the aquifer for the lowest conductance case.	A-10-14
A-10-14	Tc-99 concentrations for the lowest conductance case .	A-10-15
A-10-15	Tc-99 aquifer concentrations for the lowest conductance case .	A-10-16
A-10-16	Tc-99 peak aquifer concentrations for the lowest conductance case.	A-10-17
A-10-17	Tc-99 horizontal vadose zone concentrations for the 3-cm/year tank farm recharge rate case	A-10-19
A-10-18	Tc-99 vertical vadose zone concentrations for the 3-cm/year tank farm recharge rate case	A-10-20
A-10-19	Tc-99 peak vadose zone concentrations3-cm/year tank farm recharge rate case.	A-10-20
A-10-20	Tc-99 flux into the aquifer for the 3-cm/year tank farm recharge rate case.	A-10-21
A-10-21	Tc-99 concentration in perched water wells for the 3-cm/year tank farm recharge rate case	A-10-22
A-10-22	Tc-99 aquifer concentrations for the 3-cm/year tank farm recharge rate case .	A-10-23
A-10-23	Tc-99 peak aquifer concentration for the 3-cm/year tank farm recharge rate case.	A-10-24
A-10-24	Tc-99 horizontal vadose zone concentrations for the 39-cm/year tank farm recharge rate case	A-10-25
A-10-25	Tc-99 vertical vadose zone concentrations for the 39-cm/year tank farm recharge rate case	A-10-26
A-10-26	Tc-99 peak vadose zone concentrations for the 39-cm/year tank farm recharge rate case.	A-10-26
A-10-27	Tc-99 flux into the aquifer for the 39-cm/year tank farm recharge rate case.	A-10-27
A-10-28	Tc-99 concentration in perched water wells for the 39-cm/year tank farm recharge rate case	A-10-28
A-10-29	Tc-99 aquifer concentrations for the 39-cm/year tank farm recharge rate case .	A-10-29
A-10-30	Tc-99 peak aquifer concentration for the 39-cm/year tank farm recharge rate case.	A-10-30
A-10-31	Tc-99 horizontal vadose zone concentrations for the maximum anthropogenic recharge rate case .	A-10-31
A-10-32	Tc-99 vertical vadose zone concentrations for the maximum anthropogenic recharge rate case .	A-10-32
A-10-33	Tc-99 peak vadose zone concentrations for the maximum anthropogenic recharge rate case.	A-10-32
A-10-34	Tc-99 flux into the aquifer for maximum anthropogenic recharge rate case.	A-10-33
A-10-35	Tc-99 concentration in perched water wells for maximum anthropogenic recharge rate case .	A-10-34
A-10-36	Tc-99 aquifer concentrations for the maximum anthropogenic rate case .	A-10-35
A-10-37	Tc-99 peak aquifer concentration for the maximum anthropogenic recharge rate case.	A-10-36
A-10-38	Tc-99 aquifer concentrations for the 10-gpm preferential flow path to well ICPP-MON-A-230	A-10-38
A-10-39	Tc-99 peak aquifer concentration for the 10-gpm preferential flow path to well ICPP-MON-A-230.	A-10-39
A-10-40	Tc-99 horizontal vadose zone concentrations for the maximum service waste inventory case	A-10-41
A-10-41	Tc-99 vertical vadose zone concentrations for the maximum service waste inventory case	A-10-42
A-10-42	Tc-99 peak vadose zone concentrations for the maximum service waste inventory case.	A-10-42
A-10-43	Tc-99 flux into the aquifer for the maximum service waste inventory case.	A-10-43

A-10-44	Tc-99 concentration in perched water wells for the maximum service waste inventory case.	A-10-44
A-10-45	Tc-99 concentrations for the maximum service waste inventory case	A-10-45
A-10-46	Tc-99 peak aquifer concentration for the maximum service waste inventory case.	A-10-46
A-10-47	Subdomain model horizontal discretization.	A-10-47
A-10-48	Tc-99 horizontal vadose zone concentrations for the 50- x 50-m submodel case	A-10-48
A-10-49	Tc-99 vertical vadose zone concentrations for the 50- x 50-m submodel case	A-10-49
A-10-50	Tc-99 peak vadose zone concentrations for the 50- x 50-m submodel case.	A-10-49
A-10-51	Tc-99 flux into the aquifer for the 50- x 50-m submodel case.	A-10-50
A-10-52	Tc-99 concentration in perched water wells for the 50- x 50-m submodel case	A-10-51
A-10-53	Tc-99 aquifer concentrations for the 50- x 50-m submodel case	A-10-52
A-10-54	Tc-99 peak aquifer concentration for the 50- x 50-m submodel case.	A-10-53

LIST OF TABLES

A-3 SUMMARY OF VADOSE ZONE DATA

A-3-1	INTEC alluvium unsaturated hydraulic properties.	A-3-2
A-3-2	Basalt hydraulic conductivity from perched water tests.	A-3-3
A-3-3	INTEC interbed unsaturated hydraulic properties.	A-3-4
A-3-4	Interbed hydraulic conductivity from perched water and core tests.	A-3-5
A-3-5	Tank farm infiltration monitoring data summary.	A-3-7
A-3-6	Well summary.	A-3-18
A-3-7	OU 3-13 RI/BRA model water balance.	A-3-26
A-3-8	Current (post-remedial action) water balance.	A-3-26
A-3-9	Preliminary COPCs and partition coefficients.	A-3-28

A-4 AQUIFER DATA SUMMARY

A-4-1	HI interbed elevation and thickness data.	A-4-2
A-4-2	Snow River Plain Aquifer hydraulic conductivity values.	A-4-4
A-4-3	Summary of HI interbed permeability values.	A-4-5

A-5 VADOSE ZONE AND AQUIFER CONCEPTUAL MODELS

A-5-1	Geostatistical parameters for the nine continuous variables describing lithology.	A-5-2
A-5-2	Geostatistical parameters for the nine categorical variables based on textural class.	A-5-3
A-5-3	Simulated annual average Big Lost River infiltration rate.	A-5-9
A-5-4	Water application rates for the pre-remedial action.	A-5-11
A-5-5	Water application rates for the post-remedial action period.	A-5-13
A-5-6	OU 3-14 contaminant source locations and liquid release rate used in tank farm submodel.	A-5-14
A-5-7	Contaminant source locations and liquid release rate used in the large-scale model	A-5-15
A-5-8	Geostatistical parameters for the HI interbed thickness and elevation.	A-5-20
A-5-9	Aquifer model water sources and amounts.	A-5-24

A-7 VADOSE ZONE MODEL CALIBRATION

A-7-1	Final calibrated hydraulic parameters.	A-7-6
A-7-2	Calibrated model transport parameters.	A-7-24

A-8 AQUIFER MODEL CALIBRATION

A-8-1	Total source mass or activity used in the vadose zone and aquifer models.	A-8-3
A-8-2	Calibrated aquifer model parameters.	A-8-7
A-8-3	Calibrated aquifer model transport parameters.	A-8-10

A-9 GROUNDWATER PATHWAY RISK PREDICTION

A-9-1	Parameter values for the GWSCREEN screening analysis.	A-9-5
A-9-2	Results of radionuclide screening	A-9-7
A-9-3	Uranium isotope mass concentrations.	A-9-10
A-9-4	Results of nonradionuclide screening.	A-9-10
A-9-5	COPC source term summary.	A-9-11
A-9-6	OU 3-14 liquid releases.	A-9-12

A-9-7	Remaining OU 3-13 Sources.....	A-9-13
A-9-8	OU 3-13 contaminated soil sites.	A-9-14
A-9-9	Service waste source terms.	A-9-15
A-9-10	Contaminants of potential concern summary.....	A-9-17
A-9-11	Vadose zone simulation results.	A-9-61
A-9-12	Aquifer simulation results.....	A-9-63

A-10 ASSESSMENT OF MODEL LIMITATIONS

A-10-1	Sensitivity analysis simulations.	A-10-2
A-10-2	Vadose zone model sensitivity analysis peak concentrations.....	A-10-54
A-10-3	Aquifer model sensitivity analysis peak concentrations.	A-10-54
A-10-4	Vadose zone model sensitivity analysis calibration statistics.....	A-10-55

ACRONYMS

bgs	below ground surface
BRA	baseline risk assessment
BM	below massive (basalt flow)
CERCLA	Comprehensive Environmental Response, Compensation and Liability Act
CFA	Central Facilities Area
COC	contaminant of concern
COPC	contaminant of potential concern
CPP	Chemical Processing Plant
DEQ	Department of Environmental Quality (Idaho)
DOE	Department of Energy
EDW	Environmental Data Warehouse
EPA	U.S. Environmental Protection Agency
ESRP	Eastern Snake River Plain
FS	feasibility study
ICDF	INEEL CERCLA Disposal Facility
ICP	Idaho Cleanup Project
ICPP	Idaho Chemical Processing Plant
INEEL	Idaho National Engineering and Environmental Laboratory
INL	Idaho National Laboratory
INTEC	Idaho Nuclear Technology and Engineering Center
K _d	soil/water partition coefficient
LET&D	Liquid Effluent Treatment and Disposal (facility)
MCL	maximum contaminant level
MRDS	monitoring report/decision summary
MWTS	monitoring well and tracer study
NPL	National Priorities List

OU	operable unit
PA	performance assessment
PEW	process equipment waste
RI	remedial investigation
RI/BRA	remedial investigation/baseline risk assessment
RI/FS	remedial investigation/feasibility study
RMS	root mean square
RTC	Reactor Technology Complex
RWMC	Radioactive Waste Management Complex
SDA	Subsurface Disposal Area (at RWMC)
SRPA	Snake River Plain Aquifer
SVOC	semivolatile organic compound
TAN	Test Area North
USGS	United States Geological Survey
VOC	volatile organic compound
WAG	waste area group
WCF	Waste Calcining Facility

Groundwater Risk Pathway Model Development, Calibration and Predictive Results

A-1 INTRODUCTION

Idaho Nuclear Technology and Engineering Center (INTEC) is a large industrial complex located in the south-central portion of the Idaho National Laboratory (INL) Site. The historical mission of INTEC, formerly known as the Chemical Processing Plant [CPP]) was to recover fissile uranium by reprocessing spent nuclear fuel. The resulting liquid waste generated from this process was acidic and radioactive. The liquid contained fission products, activation products, transuranic radionuclides, and various metals. The liquid waste was temporarily stored in an underground tank farm facility located at INTEC until the liquid radioactive waste was converted to a solid granular form. Leaks and spills from piping and valves have occurred during waste transfer activities, thereby releasing contaminants to the surrounding soil. Figure A-1-1 illustrates the location of the INL Site, INTEC, and tank farm.

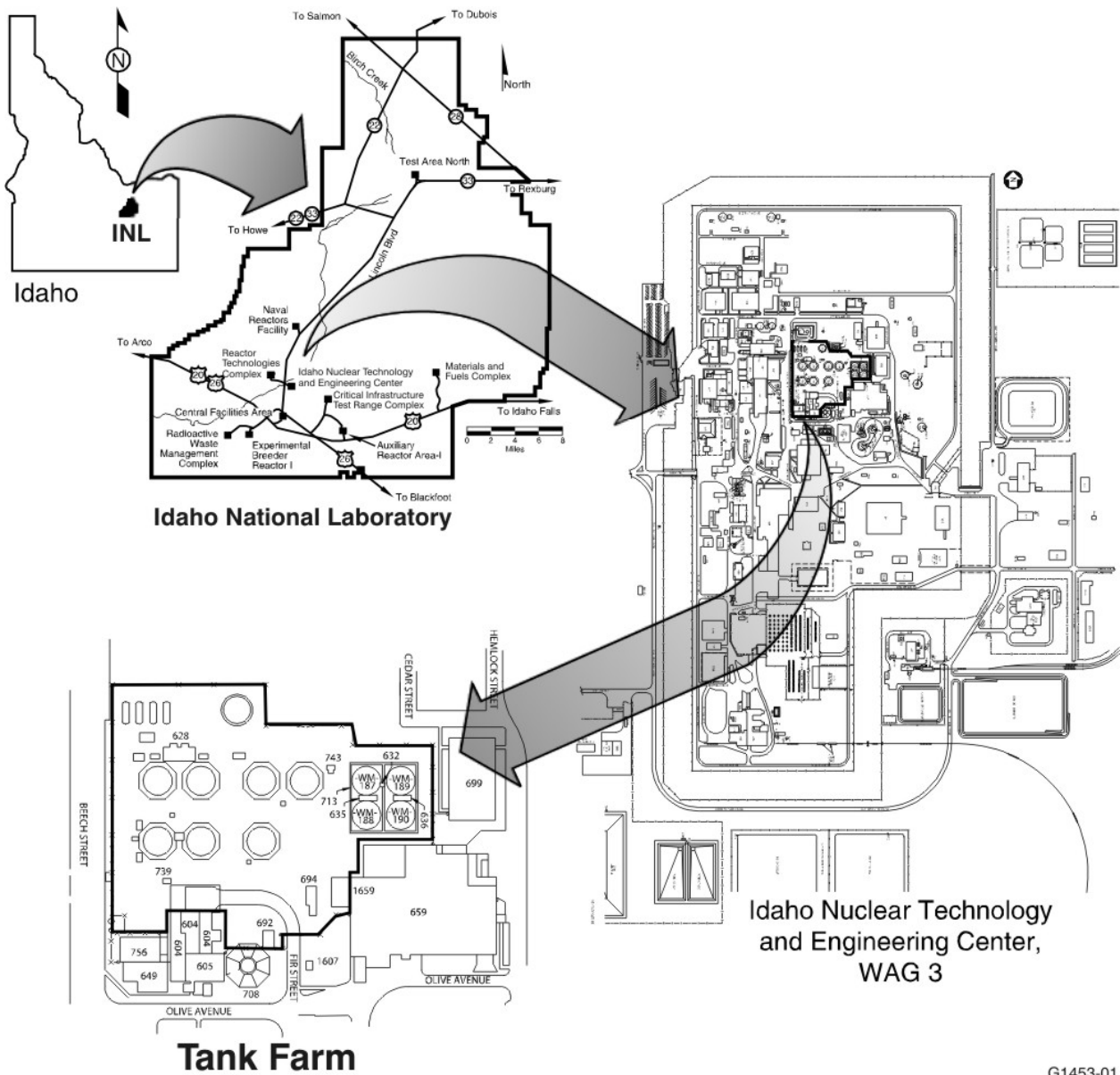
The INL Site is on the National Priority List (NPL) and is subject to the provisions of the Comprehensive Environmental Response, Compensation and Liability Act (CERCLA). The tank farm contaminated soils and groundwater are undergoing a Remedial Investigation and Feasibility Study (RI/FS) and has been designated Waste Area Group 3 (WAG 3), Operable Unit (OU) 3-14. Infiltrating water, resulting from natural and anthropogenic sources, moves down through the contaminated soil, mobilizes contaminants, and may eventually transport them to the aquifer. It is necessary to predict the future impact of the contaminated soil on the Snake River Plain Aquifer to support the RI/FS. This report documents the INTEC conceptual and numerical model, which will be used as the basis for predicting future groundwater contaminant concentrations resulting from the INTEC CERCLA releases. The groundwater concentrations are used in exposure calculations to assess risk from the groundwater ingestion pathway and to compare to regulatory groundwater concentration limits.

A-1.1 Report Organization

Simulation of flow and contaminant transport from the INTEC ground surface to the aquifer requires an understanding of the movement of water and of the chemical behavior of solutes in the subsurface. In general, the modeling process includes the following tasks: (1) definition of the modeling purpose and goals, (2) field data collection and review, (3) conceptual model development, (4) code selection, (5) conceptual model parameterization, (6) parameter adjustment to calibrate the model, (7) model sensitivity analysis, (8) prediction of aquifer concentrations, and (9) assessment of model prediction uncertainty. These tasks are presented below:

- Definition of Modeling Purpose and Goals - This task guides the entire model development because the end use of the model defines the complexity needed in the conceptual model, and the data needed to parameterize and calibrate the model. This task is presented in Section 2 along with the motivation for updating the INTEC conceptual and numerical models.
- Field Data Collection and Review - This task provides data needed for model development and identifies potential data gaps. The data available for developing the OU 3-14 groundwater models is presented for the vadose zone and aquifer in Sections 3 and 4, respectively.
- Conceptual Model Development - This task is an interpretation of collected data to understand how water and contaminants move in the subsurface. The INTEC conceptual model development has already been performed and is not presented in this Appendix, but can be found in the *Phase 1 Monitoring Well and Tracer Study Report for Operable Unit 3-13, Group 4, Perched Water* (DOE-ID 2003a).

- Code Selection - The purpose of this task is to select a software package that best answers the contaminant fate and transport simulation needs. An informal code selection task was performed and the TETRAD simulator (Vinsome and Shook 1993) was found to be the best software for simulating the unsaturated and saturated zone below INTEC. The simulation code is presented in Section 6.
- Conceptual model Parameterization - This task is performed by quantifying the conceptual model into a numerical model. The quantification requires assigning physical locations to important structures (i.e., interbeds and basalt flows) and assigning hydrologic and transport properties to these structures. The vadose zone and aquifer conceptual models and simulation methodology are presented in Section 5.
- Parameter Adjustment to Calibrate the Model - This task is performed by adjusting model hydrologic and transport parameters until simulated conditions agree with observations. It is not feasible for a numerical model, based on averaged hydrologic and transport properties, to exactly represent each field observation of vadose zone water content, perched water level, or solute concentrations. Instead the goal is to obtain the best overall match in water and solute movement. The vadose zone and aquifer model calibration were two very distinct tasks and they are presented in two sections. Section 7 presents the vadose zone model calibration process, and Section 8 presents the aquifer calibration process.
- Prediction of Aquifer Concentrations - This task uses the calibrated model to predict the future state of the system. The final model groundwater risk predictions are the basis for choosing tank farm remedial actions. The predictive results are presented in Section 9 along with identification of contaminants predicted to threaten the aquifer.
- Model Sensitivity Analysis - This task is performed to determine model sensitivity to input data. The data that results in the greatest model sensitivity can then be used to guide field data collection activities, which are the most valuable to reduce model prediction uncertainty. The results of the sensitivity analysis can also be used to guide the assessment of final prediction uncertainty. Model parameters that produce insensitive model results do not need to be included in the uncertainty analysis. The model sensitivity is presented in Section 10.
- Assessment of Model Prediction Uncertainty - Model prediction uncertainty is assessed to quantify the uncertainty in predicted future state given the uncertainty in model input data. The model uncertainty can be used to increase confidence in remedial decisions or guide further data collection activities. The assessment of model limitations (uncertainty) due to parameter sensitivity is presented in Section 10 along with the sensitivity analysis.



G1453-01

Figure A-1-1. Map showing the location of the INL Site, INTEC, and the tank farm (from Figure 1-1 of DOE-ID 2003b).

A-2 MODELING PURPOSE AND MOTIVATION

A-2.1 Purpose

The primary purposes of developing new INTEC conceptual and numerical models are to predict future concentrations of contaminants of concern (COCs) resulting from historical INTEC releases and to allow evaluation of proposed remedial actions for those COCs. The specific COCs considered here were identified in the OU 3-14 RI/FS Work Plan (DOE 2004a). The flow model parameterization is largely based on an updated geologic and hydrologic description of the subsurface relative to the previous OU 3-13 Remedial Investigation/Baseline Risk Assessment (RI/BRA) model (DOE-ID 1997). The updates are based on data collected during the 1997-2004 time frame. This model is similar to that used during the OU 3-13 RI/BRA investigation in that it considers transient three-dimensional infiltration and transport through the vadose zone, and saturated flow and transport in the aquifer. Much of the data reviewed in that document along with additional data collected during the ongoing OU 3-13 remedial activities and OU 3-14 RI/FS is used as the basis of this analysis, with primary differences occurring in the treatment of individual sedimentary interbeds, the hydraulic parameters assigned to them, and in the contaminant source releases for OU 3-14. The specific differences between the OU 3-13 and the OU 3-14 model is discussed in Section A-2.2. The simulation results will be used to

- Evaluate impacts to aquifer water quality from historical leaks and spills in the tank farm and INTEC.
- Predict concentrations in the Snake River Plain Aquifer for use in the risk assessment.
- Evaluate impacts to aquifer water quality from the non-tank-farm OU 3-13 RI/BRA (DOE-ID 1997) contamination sources along with the OU 3-14 sources. If necessary, adjust OU 3-13 sources to reflect contaminants removed during the remedial work or new information.
- Evaluate proposed remedial actions during the feasibility study phase of the OU 3-14 RI/FS.

A-2.2 Motivation

Development of an updated INTEC conceptual and numerical model was needed because data gathered during the OU 3-13 Group-4 (perched water) and Group-5 (Snake River Plain Aquifer) remedial actions and INEEL CERCLA Disposal Facility (ICDF) groundwater investigations are inconsistent with the OU 3-13 RI/BRA conceptual and numerical models (DOE-ID 1997). The OU 3-13 conceptual model grouped the many INTEC interbeds into four “effective” interbeds. This grouping simplified the vadose zone model and allowed efficient numerical simulation of the OU-13 contaminant fate and transport problem. However, the “effective” interbed structure was much more continuous than the observed structure and the simulated perched water moved a large horizontal distance. The model predicted percolation pond water would recharge the perched water beneath the tank farm. However, the INTEC vadose zone tracer test and geochemical analysis presented in DOE-ID (2003a) indicate this may not be occurring. The RI/BRA model also placed the large tank farm releases (Sites CPP-31 and CPP-28) directly into the basalt beneath the alluvium. The “effective” interbeds and placing the large tank farm releases below the alluvium may have significantly misrepresented the risk to the aquifer posed by contaminants at the tank farm. The specific differences between the OU 3-13 and OU 3-14 models are:

- OU 3-14 vadose zone model correctly simulates interbed placement and the OU 3-13 model used “effective” interbeds.
- OU 3-14 vadose zone model uses smaller grid discretization (100- x 100-m horizontal grid block vs. 200- x 200-m grid blocks).

- OU 3-14 vadose zone model was parameterized with INTEC properties versus OU 3-13 model's parameterization from SDA properties (sediment hydraulic properties and the infiltration rate).
- More data was available to parameterize and calibrate the OU 3-14 model (stratigraphy, water level and concentration data).
- OU 3-14 aquifer model correctly simulates effective aquifer thickness and aquifer surface. The aquifer depth was variable and estimated from temperature logs of deep wells (25 m to 375 m thick). The OU 3-13 model used a uniform 76-m thickness.
- OU 3-14 aquifer model uses smaller grid discretization (100- x 100-m horizontal grid block vs. 200- x 200-m grid blocks near INTEC and 2-m vertical grid block near water table and HI interbed vs. 20 m).

A-3 SUMMARY OF VADOSE ZONE DATA

Accidental releases of contaminant-bearing liquids during fuel reprocessing activities at INTEC have resulted in a long history of subsurface monitoring and characterization. Numerous historical DOE remedial investigations, DOE remediation activities, and United States Geological Survey (USGS) investigations have contributed to the subsurface transport characteristics at INTEC. In addition, the INTEC subsurface is probably the most instrumented and monitored location at the INL Site. The INTEC subsurface has been the subject of several different modeling studies, most of which were focused on integrating geologic, hydrologic, and transport data into predictive simulations. As a result of these various activities, there is a wide range of qualitative, quantitative, and interpretive information available for parameterizing this updated large-scale INTEC vadose zone flow and transport model.

A-3.1 Vadose Zone Geology and Lithology

USGS and DOE have drilled numerous wells within the vicinity of the INTEC to investigate the movement of water and contaminants. USGS has described the stratigraphy of basalt-flow groups and sedimentary interbeds in the upper 700 ft of material extending from land surface, through the vadose zone and into the aquifer. Information sources include geophysical logs, lithologic logs, and well cores. These geological cross-sections, basalt flow groups, interbed elevation maps, interbed thickness maps, and lithologic data were presented by Anderson (1991). More recent drilling activities were described in the Phase I Monitoring Well and Tracer Study Report (DOE-ID 2003a), in the ICDF drilling reports (INEEL 2003a; Cahn and Ansley 2004). The work described included drilling and installation of monitoring systems ranging from alluvium boreholes to perched water and aquifer monitoring wells. Perched water and soil samples extracted from well cores during drilling were analyzed for chemical and hydrological properties (DOE-ID 2003a). In total, USGS and DOE investigations have provided 125 wells around INTEC with 75 of those completed in the vadose zone and 49 penetrating into the SRPA.

A detailed study of the borehole data from most of these wells was completed during the preparation of the OU 3-13, Group 4, Monitoring Well and Tracer Study (DOE-ID 2003a). The study evaluated basalt/interbed core, geochemical, paleomagnetic, K-Ar age date, and petrographic data. Results of the study indicated that several distinct lithologic layers exist beneath INTEC that can be used as marker units. The marker units included the following:

- Surficial alluvium - is the uppermost sediment unit that extends from land surface. It exists across the facility, is on the order of 40 ft thick, and is underlain by fractured basalt.
- Upper basalt flows - are the numerous basalt flows between the 30- to 115-ft depth ranges from one to four flow units. Up to four units exist beneath the northern portion of INTEC while a single flow unit exists beneath the southern portion of the facility.
- 110-ft interbed - is generally encountered between 100 to 120 ft below land surface and ranges from 3 to 25 ft thick. It is an important marker unit due to its presence in nearly all of the wells penetrating deep enough to encounter it. The thickest portions of the unit rest under the northeast corner of INTEC.
- High K₂O basalt flow - is characterized by a high natural gamma count due to higher potassium content. The flow is found between 110 to 150 ft below land surface and is absent from the east and southeast extremes of INTEC. The unit lies stratigraphically below the 110-ft interbed when it is present.
- 140-ft interbed - does not appear to be as continuous as the 110-ft interbed. These predictions may reflect reality but there is uncertainty due to more limited data in the area.
- Middle massive basalt - is one of the thickest, most massive basalt flows found in the INTEC vadose

zone. Typical thickness for the unit is around 100 ft. The base of the unit appears to be relatively flat-lying while the upper surface has a south-to-southwest slope. The unit is encountered between 220 to 280 ft below land surface.

- Interbed below the middle massive basalt flow (BM interbed) - is as continuous as the 110-ft interbed and more continuous than the 140-ft interbed based on a geostatistical analysis. It ranges in thickness between 0 to 40 ft and exists below the middle massive basalt flow. This name is unique to this document and does not follow the common nomenclature of residing between a B and M basalt flow.
- 380-ft interbed - is a relatively continuous flat layer that varies in thickness from 6 to 27 ft. Depth to the interbed ranges from 320 to 420 ft below land surface. The interbed appears to be continuous and relatively thick beneath the INTEC tank farm and thin to the south.
- Low K₂O basalt flow - was identified in USGS-121 and USGS-123 at 415 ft below land surface. It has a low percentage by weight of K₂O. A similar reading from a basalt was found at 384 ft below land surface in well ICPP-COR-A-023.

In addition to the data provided by Anderson (1991) and DOE-ID (2003a), well logging information was also obtained from the INL's Hydrogeologic Data Repository (HDR) to construct the complete lithologic database of the INTEC subsurface. Interpretation of the lithologic data for the purposes of simulation was provided in Appendix C and is reviewed in Section A-5.1.4.1.

A-3.2 Vadose Zone Hydrological Data

Hydrologic data available for the INTEC vadose zone include soil moisture characteristics, particle size distribution, porosity, effective porosity, bulk density, and moisture content. These data are available from a variety of sources including Appendix F of the OU 3-13 RI/BRA (DOE-ID 1997) and the OU 3-13, Group 4, remedial activities (DOE-ID 2003a). The former document reviews the results of perched water tests, and the latter reviews the analysis of core samples collected during drilling of perched water wells at the INTEC. The OU 3-13, Group 4, remedial work collected a total of 37 surficial alluvium and interbed samples during Phase I drilling. The laboratory analysis developed soil moisture characteristic curves and determined material particle size distribution, porosity, effective porosity, bulk density, and initial moisture content. These data are presented in the next three subsections for the alluvium, basalt, and interbed, respectively.

A-3.2.1 Surficial Alluvium

The INTEC alluvium ranges in thickness from 22 to 61 ft near INTEC and varies in texture from inorganic clays and silts to well-sorted gravel, but it is primarily poorly graded gravel and sand mixtures. Hydraulic properties for 17 samples of alluvium were obtained during the OU 3-13, Group 4, remedial activities using laboratory core analysis and are presented in Table A-3-1.

Table A-3-1. INTEC alluvium unsaturated hydraulic properties from DOE-ID (2003a).

Well Name	Depth	Unified Soil Class	Dry Bulk Density	Saturated Hydraulic Conductivity	van Genuchten Parameters		Volumetric Moisture Content		
					Alpha (1/cm)	N	In Situ	Residual	Saturated
(ICPP-SCI-P-)	(ft)		(g/cm ³)	(cm/sec)					
216	33-34	GW-GM	1.8	4.80E-02	1.9868	1.2407	0.066	0.026	0.2555
216	34-35	GM	1.3	1.10E-01	1.2729	1.1024	0.21	1.00E-04	0.4198

Well Name	Depth	Unified Soil Class	Dry Bulk Density	Saturated Hydraulic Conductivity	van Genuchten Parameters		Volumetric Moisture Content		
(ICPP-SCI-P-)	(ft)		(g/cm ³)	(cm/sec)	Alpha (1/cm)	N	In Situ	Residual	Saturated
226	10-10.5	GW-GM	2.01	6.90E-02	0.3126	1.2521	0.117	0.0256	0.2864
226	19-20	GP	2.16	7.40E-03	0.1123	1.5444	0.097	0.0516	0.2247
226	45-46	SM-SC	1.79	6.60E-07	0.0163	1.1881	0.223	1.00E-04	0.401
226	51-52	ML-CL	1.95	6.70E-08	0.0002	1.3428	0.379	1.00E-04	0.3851
248	10-10.5	GP	1.78	3.80E-02	0.1723	1.4687	0.048	0.0326	0.3321
248	18-18.5	GP-GM	1.68	4.70E-02	0.0467	2.0252	0.053	0.0602	0.3696
250	15-15.5	GW	1.7	8.00E-02	0.0124	2.3011	0.062	0.0316	0.2354
250	26-26.5	GP	1.67	1.00E-01	0.2086	1.3291	0.095	0.0144	0.3745
250	31-31.5	GP-GM	1.61	1.60E-02	0.3134	1.2618	0.11	0.0192	0.3923
251	19-19.5	GP	2	3.00E-02	0.0197	4.2289	0.081	0.0622	0.3142
251	19-19.5	GW	1.9	2.70E-02	0.123	1.327	0.102	0.0265	0.3477
251	30.5-31	GP-GM	1.82	1.70E-02	1.5208	1.1435	0.103	1.00E-04	0.2677
252	20-23	GP	1.89	5.60E-02	0.7955	1.2084	0.087	1.00E-04	0.321
252	26-27	GW	1.99	4.40E-02	0.0861	1.914	0.085	0.0642	0.2518
252	41-42.5	GP-GM	1.88	6.10E-02	0.159	1.5421	0.087	0.0432	0.2939

A-3.2.2 Vadose Zone Basalt

The geology of the Eastern Snake River Plain is the result of plains-style, low-shield volcanoes. The basalt flows are episodic, and during quiescent periods, sediments are deposited over the basalt. The basalt flows typically have five layered elements consisting of a fractured and fissured base surface followed by a sequence of a rubble zone, lower vesicular zone, massive center, and upper vesicular zone (Knutson et al. 1990).

Direct measurements of unsaturated hydraulic characteristics are unavailable for the highly heterogeneous basalts. However, saturated hydraulic conductivity is available for the perched water tests conducted at INTEC. These results are reproduced in Table A-3-2 from Appendix F of the OU 3-13 RI/BRA (DOE-ID 1997).

Table A-3-2. Basalt hydraulic conductivity from perched water tests from DOE-ID (1997).

Well	Depth (ft bls)	Test Type	Material	Hydraulic Conductivity (cm/sec)
CPP 33-2	97.8-105.8	Pumping/recovery	Basalt	1.80E-03
CPP 33-3	111.2-121.8	Pumping/recovery	Basalt	9.50E-04

Well	Depth (ft bls)	Test Type	Material	Hydraulic Conductivity (cm/sec)
CPP 33-4	103.7-118.2	Pumping/recovery	Basalt	2.40E-03
CPP 33-4	103.7-118.2	Pumping/recovery	Basalt	3.40E-03
CPP 55-6	105.2-113.1	Pumping/recovery	Basalt	4.20E-04

A-3.2.3 Interbeds

The sedimentary interbeds at INTEC consist of fluvial, lacustrine, and eolian deposits of clay, silt, sand, and gravel, which have accumulated during quiescent periods between basalt flows (Anderson 1991). There are between 15 to 20 sedimentary interbeds beneath INTEC, depending on location. However, as reviewed in Section A-3.1, the OU 3-13, Group 4, Monitoring Well and Tracer Study (MWTS) report (DOE-ID 2003a) suggests there are only four significant interbeds. These are the (1) 110-ft interbed, which is 3 to 25 ft thick and encountered 100 to 120 ft below land surface; (2) 140-ft interbed, which is discontinuous; (3) the interbed below the middle massive basalt unit (BM interbed); and (4) the 380-ft interbed, which is 6 to 27 ft thick and is encountered 320 to 420 ft below land surface.

Appendix F of the OU 3-13 RI/BRA (DOE-ID 1997) included the results of the perched water tests conducted in interbed zones and laboratory analysis of core samples. The OU 3-13, Group 4, remedial work included laboratory analysis of 20 interbed core samples. These data and the data from the OU 3-13 RI/BRA are presented in Tables A-3-3 and A-3-4, respectively.

Table A-3-3. INTEC interbed unsaturated hydraulic properties from DOE-ID (2003a).

Well Name	Depth	Unified Soil Class	Dry Bulk Density	Saturated Hydraulic Conductivity	van Genuchten Parameters		Moisture Content		
					Alpha (1/cm)	N	Iin Situ	Residual	Saturated
(ICPP-SCI-P-)	(ft)		(g/cm ³)	(cm/sec)					
248	87-87.5	ML-MC	1.39	1.00E-06	0.0006	1.2776	0.456	0	0.4799
248	167.6-168.3	ML	1.43	4.60E-05	0.0045	1.2501	0.333	0	0.4533
248	167.6-168.3	ML	1.29	4.70E-04	0.0158	1.1925	0.358	0	0.44
249	376-377.5	SM	1.53	2.50E-06	0.0008	1.3951	0.445	0	0.394
249	381.8-382.8	SM	1.8	8.00E-04	0.0851	1.1797	0.261	0	0.3138
249	387.1-388.2	ML	1.32	9.90E-04	0.0509	1.1683	0.285	0	0.5238
249	387.1-387.2	ML	1.53	7.50E-07	0.0007	1.2883	0.383	0	0.434
249	164.2-164.7	ML	1.37	7.80E-04	0.0003	1.3161	0.331	0	0.3921
250	110.8-111.45	SM	1.08	3.30E-02	0.105	1.2886	0.266	0.0685	0.6024
250	122.2-122.9	ML	1.46	3.10E-04	0.0021	1.4487	0.422	0.0447	0.4758
250	132.7-133.1	ML	1.51	2.40E-04	0.0023	1.2575	0.399	0	0.4724
250	168-173.3	SM	1.19	4.40E-03	0.0972	1.1932	0.339	0	0.517

Well Name	Depth	Unified Soil Class	Dry Bulk Density	Saturated Hydraulic Conductivity	van Genuchten Parameters		Moisture Content		
(ICPP-SCI-P-)	(ft)		(g/cm ³)	(cm/sec)	Alpha (1/cm)	N	I _{in Situ}	Residual	Saturated
250	170-170.9	SM	1.23	8.20E-04	0.0266	1.2199	0.339	0	0.5109
250	384-385.1	SM	0.92	1.50E-02	1.6681	1.1352	0.207	0	0.5625
250	384-384.4	ML	1.33	4.60E-07	0.0001	2.1085	0.338	0.0764	0.4442
251	103-103.8	SM	1	2.80E-02	0.2005	1.1726	0.268	0	0.6049
251	108.3-109.5	ML	1.31	4.20E-03	0.0076	1.1638	0.366	0	0.4847
251	114-114.7	CL	1.4	2.50E-07	0.0001	1.3795	0.464	0	0.4934
252	144.6-152.2	SM	1.13	8.10E-03	0.1212	1.1666	0.275	0	0.5116
252	154.5-156.2	ML	1.51	8.20E-07	0.0003	1.3471	0.322	0	0.4226

Table A-3-4. Interbed hydraulic conductivity from perched water and core tests from DOE-ID (1997).

Well	Material	Hydraulic Conductivity (cm/sec)	Depth (ft bls)	Test Type
MW-2	Sandy clay interbed	3.7E-3	107.9-112.0	Aquifer slug
MW-4	Silty sand and gravel interbed	3.86E-5	104.6-110.6	Aquifer slug
MW-6	Silty sand, fine grained interbed	1.3E-3	140.0-151.0	Aquifer slug
MW-3	Silty clay	8.9E-5	117.0-119.3	Laboratory core
MW-4	Silty sand and gravel	1.6E-5	108.0-109.3	Laboratory core
MW-7	Silt with fine gravel	1.3E-3	113.5-114.5	Laboratory core
MW-8	Clay with silt	1.1E-5	122.3-123.7	Laboratory core
MW-10	Sandy silt	1.0E-5	110.3-111.0	Laboratory core
MW-11	Silty sand	1.2E-5	113.7-115.3	Laboratory core
MW-4	Silt	3.2E-5	105.1-105.6	Laboratory core
MW-4	Silt	6.7E-5	105.6-106.8	Laboratory core
MW-6	Clay	3.0E-7	110.0-111.0	Laboratory core
MW-9	Clay with silt	2.1E-3	111.6-112.5	Laboratory core
MW-11	Clay	5.2E-8	135.4-136.0	Laboratory core
MW-3	Silty clay	8.3E-4	138.0-139.0	Laboratory core
MW-6	Silty clay	2.2E-3	142.0-143.0	Laboratory core

Well	Material	Hydraulic Conductivity (cm/sec)	Depth (ft bls)	Test Type
MW-9	Silt with clay	3.4E-4	148.7-149.4	Laboratory core
MW-1	Sand with silt	3.3E-4	231.7-232.3	Laboratory core

A-3.3 Vadose Zone Infiltration from Precipitation

Infiltration is the process by which surface water enters the soil. After surface water has infiltrated into the soil, it is redistributed in response to gravity and capillary forces. The redistribution process ultimately partitions the infiltrated water into (1) surface losses to evaporation and transpiration, (2) drainage that eventually becomes aquifer recharge, and (3) storage that remains in the vadose zone. Infiltrating water moves down through the contaminated soils, mobilizing contaminants, and eventually transports them to the aquifer. The storage or residual moisture is important because it determines the amount of water in contact with soil, which affects the sorption characteristics. Determination of net infiltration is primarily accomplished by analyzing field data using numerical models. One of the analyses available was performed near INL's Subsurface Disposal Area (SDA), and was used in the OU 3-13 RI/BRA, and the more relevant and recent study was conducted at the INTEC and is described in detail in Appendix B.

Infiltration values used in the OU 3-13 RI/BRA (DOE-ID 1997) were based on a USGS study (Cecil et al. 1992) for undisturbed and vegetated conditions and were based on field data representative of disturbed soils collected in the SDA (Martian 1995). Undisturbed conditions were assumed to exist outside the INTEC fence line where a value of 1 cm/year (Cecil et al. 1992) was applied. Disturbed conditions were assumed inside the INTEC fence line where 10 cm/year (Martian 1995) were applied. The 10-cm/year rate was based on moisture content and soil tension data collected over several years and at several SDA locations. Evaporation, infiltration, and storage parameters were estimated through model calibration. The infiltration behavior varied widely between monitoring locations with the primary mechanism for recharge identified as infiltration following the spring snowmelt. The fast snowmelt during periods of low evapotranspiration allowed a large percentage of the annual precipitation to become recharge even though the total potential evapotranspiration at the SDA is several times the annual precipitation. These recharge rates may not be appropriate for the tank farm because recharge resulting from precipitation is strongly dependent on soil type, topography, and surface vegetation type, which differ between the tank farm and the SDA.

Infiltration in the tank farm was investigated during 1993 and 1994. The investigation measured soil moisture content using a neutron moisture probe at 20 locations near and within the tank farm during December 1993 and early spring 1994 (INEL 1995). This time period included dry and wet periods, with data collected approximately monthly (dates provided in Table A-3-5). Although these data are more representative of INTEC than the SDA values, we note that (1) the recorded 6.3 in. of precipitation during 1994 was less than the long-term average INTEC precipitation of 8.3 in. per year and (2) irregular and infrequent sampling made it difficult to uniquely determine infiltration parameters. Additional uncertainty is introduced in the neutron probe calibration which used a standard calibration curve for Schedule 80 stainless-steel casing and moisture in a "standard block". The calibration was verified by comparing neutron probe-measured soil moisture data at two locations to laboratory-measured soil moisture from the same location. The overall ratio between probe- and laboratory-measured moisture content was 1:0.92. While introducing some uncertainty, this calibration was thought to be adequate for the tank farm soil and was used for all measurements.

In addition to these 20 sample locations, the 1993-1994 tank farm investigation also included two small-scale infiltration tests designed to determine the extent of lateral versus vertical migration. A secondary objective was to determine the sampling frequency required to observe wetting front propagation through the vadose zone. The first test used an infiltration basin emplaced around neutron probe monitoring well A-67. The basin inner radius was 7 ft from the well, the outer radius was 15.8 ft from the well, and the basin was filled to a 3.8 in. depth. The neutron probe was monitored for 72 hours. Water was never seen in the well and it was concluded that water moved vertically through the alluvium with very little lateral movement. A similar test

was conducted using a 10-ft-radius infiltration pond placed around well A-68. The basin was also filled to a 3.8 in. depth and was monitored for 72 hours. The wetting front reached the basalt interface within 40 hours. The rapid movement of the wetting front through the alluvium indicated that monitoring intervals of at least twice daily would be needed to observe wetting front movement following a period of significant precipitation.

In Appendix B, the soil moisture data and numerical calibration for 14 locations within and near the tank farm are presented. These data include samples beneath and adjacent to the membrane liner overlying the tank farm. The calibration was performed in a manner analogous to the Martian (1995) SDA infiltration study. Soil hydraulic properties were estimated by matching variable-depth and transient moisture content measurements at each location. Initial values during the calibration were taken from the OU 3-13, Group 4, characterization work (DOE-ID 2003a). The calibrated infiltration models were then used to simulate infiltration into the tank farm soil and underlying basalt for the entire historical operational period of INTEC (1953-2003). The simulations suggest that approximately 18-cm/year pass through the tank farm soil. This is a very large percentage (86%) of the approximately 21-cm/year annual total precipitation. As with the SDA data, the INTEC recharge is highly seasonal with much of the recharge resulting from spring snowmelt and rainfall. The simulated aquifer recharge at wells located beneath the liner was spatially variable with some locations experiencing higher or lower recharge rates than locations away from the liner. However, the average recharge rate for all locations beneath the membrane was nearly the same as the average rate for locations outside of the lined area. It appears as though the liner covering the tank farm redistributes infiltration and that it does not significantly change the overall recharge rate.

A very high net infiltration percentage of precipitation is not consistent with observed annual drainage percentages seen at the Hanford Field Lysimeter Test Facility (Gee et al. 1993). The highest observed drainage out of a gravel surface lysimeter was as 83% of the precipitation/irrigation treatment. Drainage percentages would be expected to be higher at the INL Site because the Site generally has a lower potential evapotranspiration rate than the Hanford Site and the INL Site's soil remains frozen for longer periods of time during winter months. Frozen soil will greatly reduce soil moisture evaporation during the winter.

More frequent monitoring of the tank farm soil moisture during the 1994 monitoring period would have improved confidence in the model calibration because many more infiltration events would have been captured in the monitoring. However, the uncertainty in the predictions is acceptable because of the following reasons: (1) a numerical model was used to estimate the total net infiltration rate, (2) the model used the complete historical weather record for the INTEC (1953-2003), and (3) the model accurately mimicked the events seen in the data. The net infiltration rate cannot be estimated from the observed data alone, because a large fraction of the infiltration events were not seen in the infrequent monitoring.

Table A-3-5. Tank farm infiltration monitoring data summary.

Well	Total Monitored Depth (ft)	Monitoring Dates
A-60	32	12/8/93, 1/28/94, 2/28/94, 4/11/94, 5/11/94
A-61	34	12/8/93
A-62	36	12/8/93, 1/28/94, 3/1/94, 4/11/94, 5/11/94
A-63	36	3/1/94, 4/11/94, 5/11/94
A-64	35	12/8/93, 1/28/94, 3/1/94, 4/11/94, 5/11/94
A-65	30	12/7/93, 1/28/94, 3/1/94, 4/11/94, 5/11/94
A-66	35	12/7/93
A-67	37	12/7/93, 1/28/94, 3/1/94, 3/31/94, 5/11/94
A-68	30	12/7/93, 1/28/94, 3/1/94, 3/31/94, 5/11/94

Well	Total Monitored Depth (ft)	Monitoring Dates
81-02	28	12/8/93, 1/28/94, 2/28/94, 4/11/94
81-04	15	2/28/94, 4/11/94, 5/11/94
81-05	13	2/28/94, 4/11/94, 5/11/94
81-06	27	4/11/94, 5/11/94
81-09	22	4/11/94, 5/11/94
81-10	28	12/8/93, 1/28/94, 2/28/94, 4/11/94, 5/11/94
81-15	11	12/8/93, 1/28/94, 2/28/94, 4/11/94
81-17	17	12/8/93, 1/28/94, 2/28/94, 4/11/94, 5/11/94
81-19	23	4/11/94, 5/11/94
81-20	28	4/11/94, 5/11/94
81-21	11	12/8/93, 1/28/94, 4/11/94, 5/11/94

A-3.4 Perched Water Depth and Soil Moisture/Tension

There are several discontinuous perched water zones beneath INTEC associated with the alluvium/basalt interface, the shallow primary interbeds at 110 ft and 140 ft, the below massive basalt (BM) interbed at 220-280 ft, and the deep interbed at 380 ft. Perched water appears to also be associated with low-permeability basalt and numerous other thin and discontinuous interbeds. For the purposes of discussion, the perched zones have been grouped into shallow, deep, and middle zones:

- The shallow perched water occurs in the northern and southern regions of INTEC, while the central area of the INTEC does not appear to have significant shallow perched water (DOE-ID 2003a). The northern shallow perched water can be divided into two principal zones associated with the 110-ft and 140-ft interbeds, respectively. Shallow perched water has been identified beneath two separate areas of southern INTEC. A small perched water body has been identified in the vicinity of Building CPP-603, and a larger perched water body has developed from the discharge of wastewater to the former percolation ponds. The larger perched water body began rapidly draining when use of the percolation ponds was discontinued in August 2002.
- The deep perched water appears to be primarily associated with the 380-ft interbed. The top of this interbed occurs beneath the western portion of INTEC at depths ranging from 375 to 426 ft below land surface (bls). Water has been encountered in the northern deep zones at approximately 322, 407, and 383 ft bls. The sources of recharge to the western portion of the northern deep perched water are unknown, although the Big Lost River and facility water leaks are likely contributors.
- An intermediate perched water zone appears at approximately 250 ft below land surface south of INTEC near the ICDF, and recharge was most likely from the former percolation pond. Recent data indicate that it has also been draining since the percolation ponds were discontinued (Cahn and Ansley 2004).

The sources of the perched water include recharge from the BLR, infiltration from the former percolation ponds, precipitation, and other anthropogenic water.

Historically, the perched water has been monitored by USGS and by DOE. Many of the wells were installed prior to the OU 3-13 RI/FS or during the OU 3-13 RI/FS. As a result of the OU 3-13 ROD

(DOE-ID 1999) institutional controls were implemented in 2002. These institutional controls include reducing the surface infiltration and monitoring resultant soil moisture and COC concentrations. The primary reduction in surface infiltration occurred when the percolation ponds were moved approximately 2 miles west of the INTEC facility on August 26, 2002. Prior to removal, the percolation ponds discharged in excess of 1 M gal of wastewater per day and accounted for approximately 70% of the known water recharging the aquifer near INTEC.

To record the transient effects resulting from moving the ponds and to reduce the overall uncertainty, the OU 3-13, Group 4, activities (DOE-ID 2003a) added several well sets around the Big Lost River, sewage treatment lagoons, and percolation ponds. These additional wells included piezometers to monitor perched water elevations, suction lysimeters to collect samples from the unsaturated zone, tensiometers to measure matric potential, and temperature sensors. Soil moisture sensors were installed in some initial wells, but were excluded from subsequent wells because of instrument failures. The Group 4 remedial wells included the following sets:

- Big Lost River (BLR) set. The BLR set is located south of the Big Lost River and was installed to monitor the northern perched water levels and to examine hydraulic connections between northern perched water and the Big Lost River.
- Sewage Treatment Lagoon (STL) set. The STL set is located west of the sewage treatment lagoons and was installed to define the perched water thickness and provide data on the hydraulic connection between the northern perched water and the sewage treatment lagoons.
- Percolation Pond (PP) set. The PP set is located north of the former percolation ponds. These wells were installed to monitor the upper and lower perched zones in the southern INTEC, to identify the hydraulic connection between the former percolation ponds and the southern perched water, and to provide monitoring points for the percolation pond tracer test.
- Tank Farm (TF) set. The TF set is located north of the tank farm and was installed to identify the effects of the Big Lost River on soil moisture and perched water at the alluvium/basalt interface, upper northern perched water, lower northern perched water, and the SRPA.
- Central Set (CS). The CS wells are located between the northern and southern upper perched water. These wells were installed to monitor conditions between the former percolation ponds and the tank farm.

Each of the well sets contained four to five well completions and were designed to collect specific data. The corehole (CH) completions were installed to collect soil and basalt core and monitor perched water. The alluvial (AL) completions were installed to monitor perched water at the alluvium/basalt interface. The shallow perched (SP) completions are monitored in the shallow perched water associated with the 110-ft to 140-ft interbeds. The deep perched (DP) completions targeted the deep perched zones at approximately 380-ft bls. Tensiometers and lysimeters were installed at various depths to monitor unsaturated conditions.

In addition to the OU 3-13, Group 4, wells, the ICDF construction project increased the monitoring network. In 2002, the ICDF installed six new perched water wells with multiple completions at varying depths (total of 15 completion intervals). Well locations for both groups are shown in Figure A-3-1. All of the perched water well locations and hydrographs are illustrated in Figures A-3-2 through A-3-8. In general, they are ordered by depth and increasing north to south direction. Data types, dates, and depths for all the wells are given in Table A-3-6.

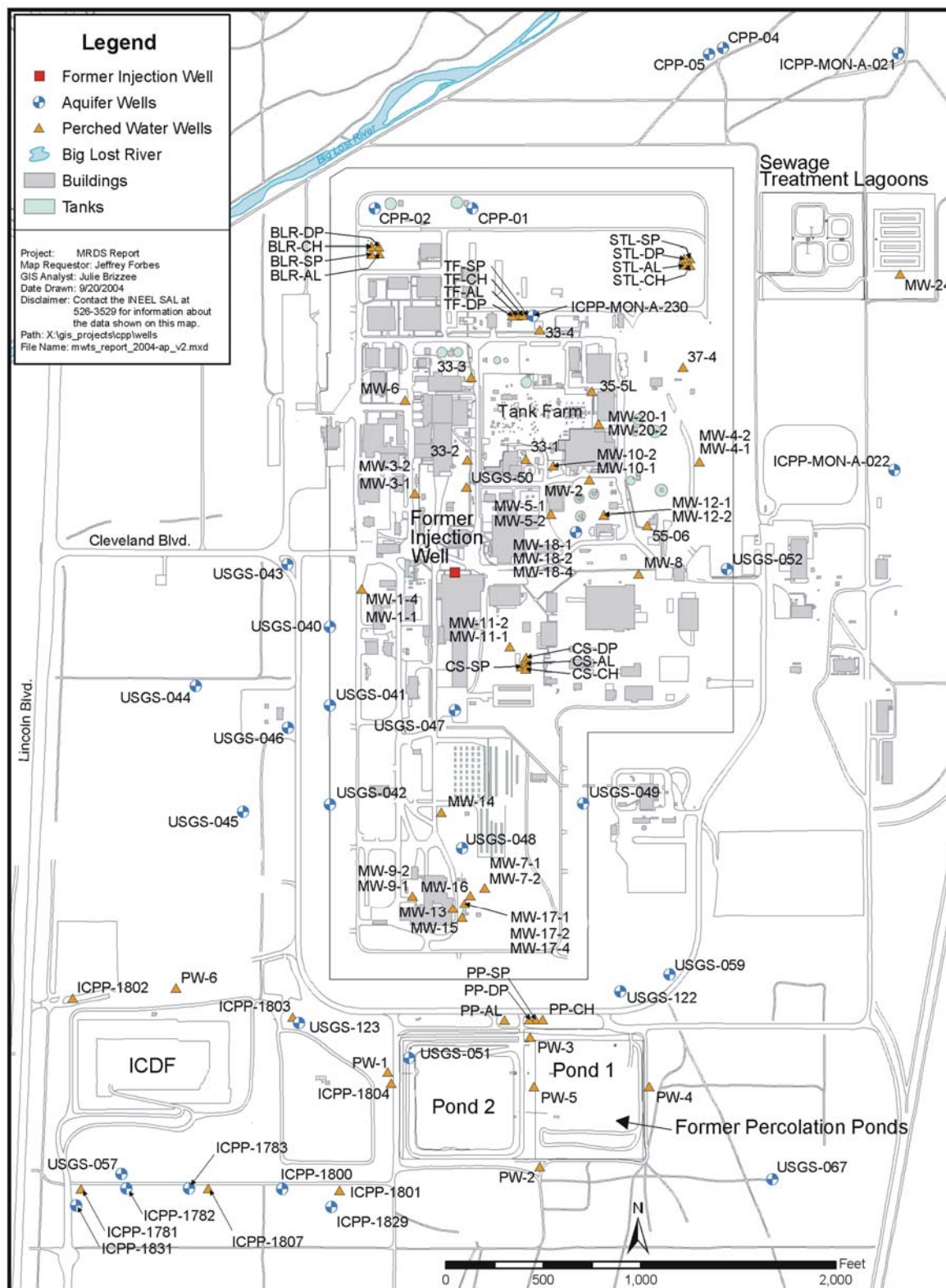
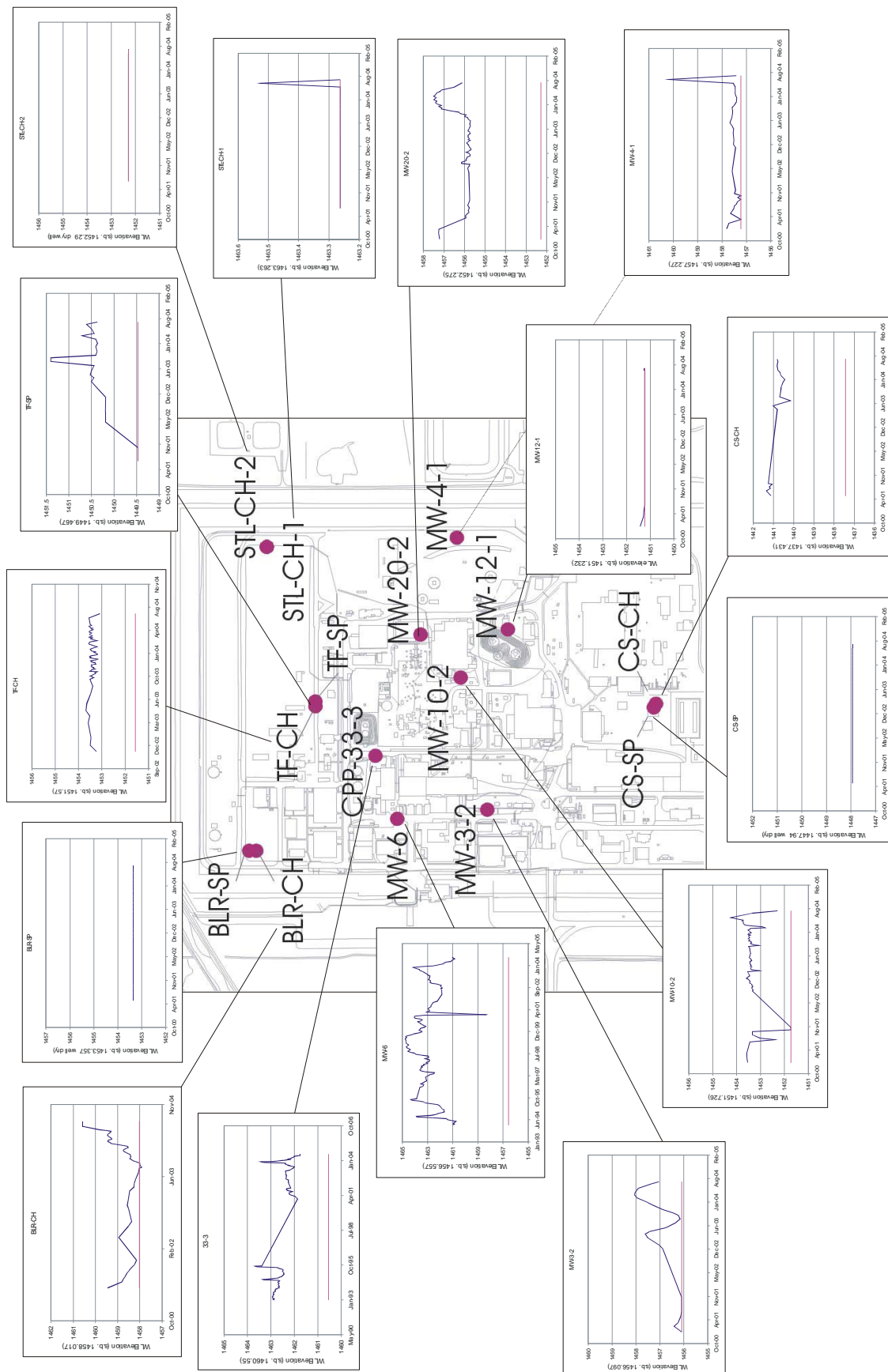


Figure A-3-1. Aquifer and perched water well locations.



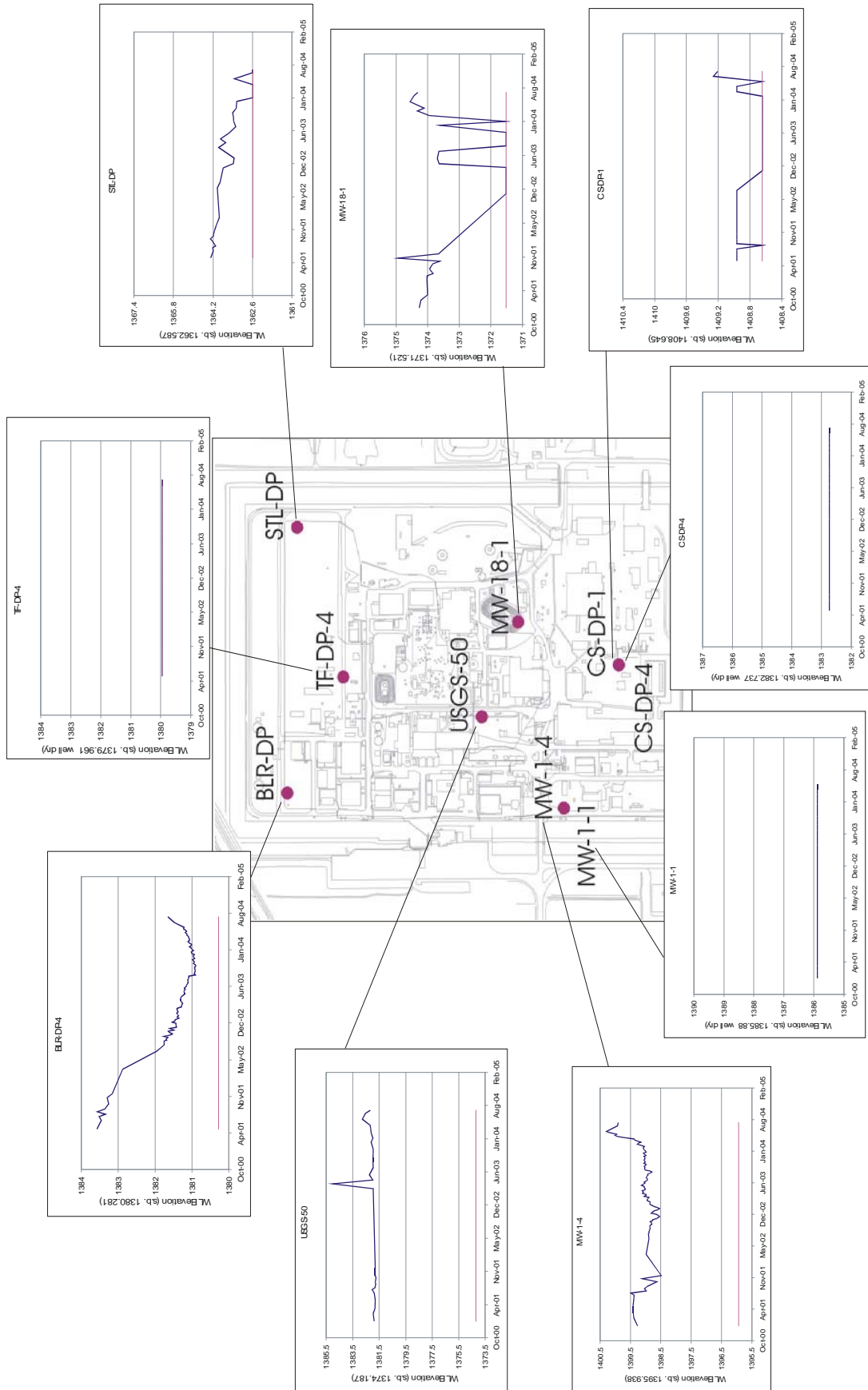
* Water level (WL) elevations and screen bottoms (s.b.) in meters.

Figure A-3-2. Alluvium perched water well locations and hydrographs.



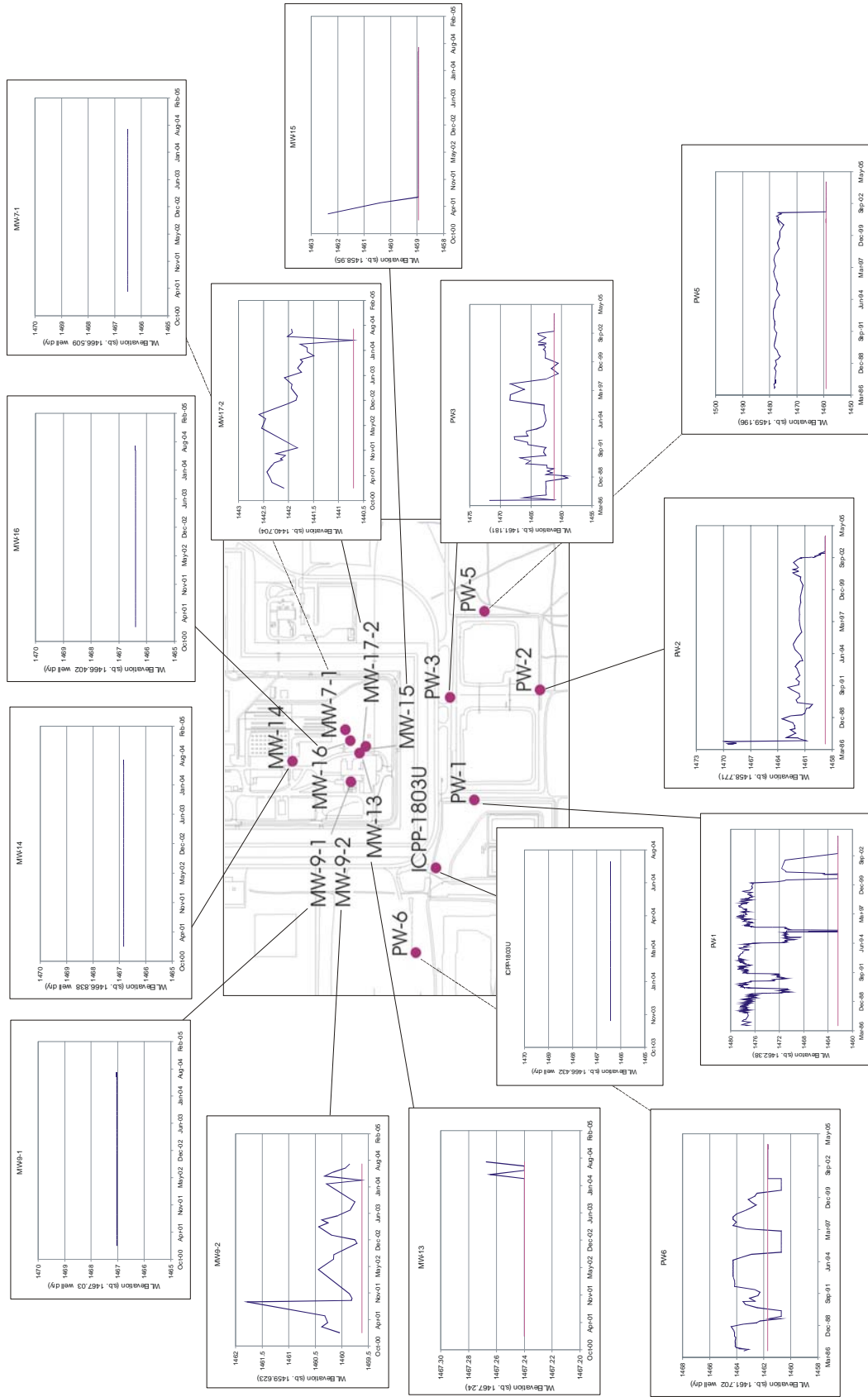
* Water level (WL) elevations and screen bottoms (s.b.) in meters.

Figure A-3-4. Northern lower shallow perched water well locations and hydrographs.



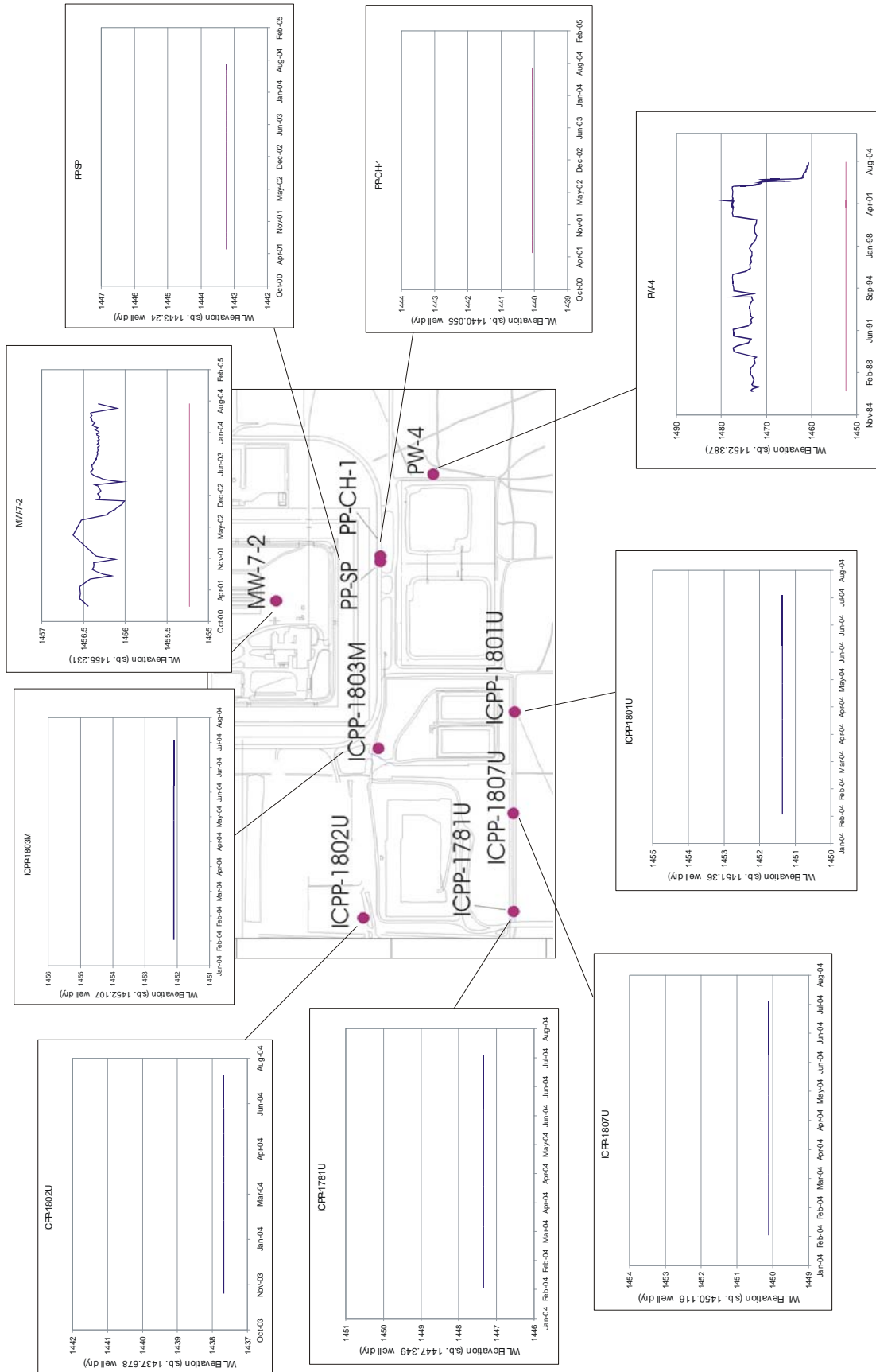
* Water level (WL) elevations and screen bottoms (s.b.) in meters.

Figure A-3-5. Northern deep perched water well locations and hydrographs.



* Water level (WL) elevations and screen bottoms (s.b.) in meters.

Figure A-3-6. Southern upper shallow perched water well locations and hydrographs.



* Water level (WL) elevations and screen bottoms (s.b.) in meters.

Figure A-3-7. Southern lower shallow perched water well locations and hydrographs.



Figure A-3-8. Southern deep perched water well locations and hydrographs.

Table A-3-6. Well summary.

Well ID	Well Name	Well Alias	Land Surface Elevation (ft)	Instrument (Depth from Land Surface) (ft)	Available Data
1428	ICPP-SCI-P-216	BLR-AL	4913.64	Lysimeter (32.3) Tensiometer (32.87) Piezometer (35.4-35.9)	August 2001-Present Automated Data Dry
1429	ICPP-SCI-P-217	BLR-SP	4913.73	Lysimeter (166.38) Tensiometer (132.5, 166.75) Piezometer (140-145.5)	August 2001-Present Automated Data Dry
1430	ICPP-SCI-P-218	BLR-DP	4913.48	Lysimeter (351.5) Tensiometer (352, 395) Screen (375-385) Screen (375-385)	August 2001-Present Automated Data September 2002-Present Automated Data April 2001-Present Manual Measurement
1444	ICPP-SCI-P-248	BLR-CH	4913.52	Screen (120-130)	April, 2001-Present Manual Measurement
1431	ICPP-SCI-P-219	STL-AL	4909.31	Lysimeter (26) Tensiometer (26.5) Piezometer (30.4-30.9)	August 2001-Present Automated Data Dry
1432	ICPP-SCI-P-220	STL-SP	4909.44	Lysimeter (103.25) Tensiometer (103.5, 146)	August 2001-Present Automated Data
1433	ICPP-SCI-P-221	STL-DP	4909.43	Lysimeter (418) Tensiometer (384.5, 416) Screen (429-439)	August 2001-Present Automated Data April 2001-Present Manual Measurement
1447	ICPP-SCI-P-251	STL-CH	4909.73	Piezometer (99-109) Screen (140-145)	June 2001-Present Manual Measurement Dry
1434	ICPP-SCI-P-222	PP-AL	4916.76	Lysimeter (26.6) Tensiometer (27.4) Piezometer (30.8-31.3)	August 2001-Present Automated Data January 2001-Present Manual Measurement
1435	ICPP-SCI-P-223	PP-SP	4917.04	Lysimeter (108.3, 168.5) Tensiometer (108.8, 131.5, 169) Piezometer (180-182)	August 2001-Present Automated Data Dry
1436	ICPP-SCI-P-224	PP-DP	4917.06	Lysimeter (382.5) Tensiometer (263.5, 383) Piezometer (50-55) Piezometer (50-55) Screen (372-382)	August 2001-Present Automated Data August 2001-Present Automated Data April 2001-Present Manual Measurement April 2001-Present Manual Measurement
1446	ICPP-SCI-P-250	PP-CH	4916.59	Piezometer (187-192) Screen (235-255)	August 2002-Present Automated Data April 2001-Present Manual Measurement

Well ID	Well Name	Well Alias	Land Surface Elevation (ft)	Instrument (Depth from Land Surface) (ft)	Available Data
1443	ICPP-SCI-P-247	CS-AL	4914.48	Lysimeter (41) Tensiometer (41.5) Piezometer (45.5-46)	August 2001-Present Automated Data Dry
1437	ICPP-SCI-P-225	CS-SP	4914.46	Lysimeter (121.5, 154.5) Tensiometer (122, 155) Piezometer (159-164)	August 2001-Present Automated Data Dry
1438	ICPP-SCI-P-226	CS-DP	4914.54	Lysimeter (279.5) Tensiometer (280, 287, 383) Piezometer (288.5-293) Piezometer (288.5-293) Screen (368-378)	August 2001-Present Automated Data July 2001-Present Automated Data April 2001-June 2002 Manual Measurement Dry
1445	ICPP-SCI-P-249	CS-CH	4914.48	Screen (188.5-198.5)	April 2001-Present Manual Measurement
1439	ICPP-SCI-P-227	TF-AL	4912.43	Lysimeter (34.5) Tensiometer (35) Piezometer (37.5-38)	August 2001-Present Automated Data Dry
1440	ICPP-SCI-P-228	TF-SP	4912.22	Lysimeter (117.5, 156.4) Tensiometer (118, 157, 173) Piezometer (145-150)	August 2001-Present Automated Data March 2002-Present Manual Measurement
1441	ICPP-SCI-P-229	TF-DP	4912.43	Lysimeter (385) Tensiometer (350.5, 388.5) Screen (375-385)	August 2001-Present Automated Data Dry
1442	ICPP-SCI-P-230	TF-Aquifer	4912.41	Screen (443-483)	September 2001-Present Manual Measurement
1448	ICPP-SCI-P-252	TF-CH	4912.36	Screen (145-150)	March 2002-Present Manual Measurement
1781	ICPP-1781	ICPP-1781	4925.99	Screen (155-175, 279-299, 375-395)	February 2004-Present Manual Measurement
1801	ICPP-1801	ICPP-1801	4921.92	Screen (138-158, 247-267)	February 2004-Present Manual Measurement
1802	ICPP-1802	ICPP-1802	4925.12	Screen (186-206, 291-311, 363-383)	November 2003-Present Manual Measurement
1803	ICPP-1803	ICPP-1803	4921.99	Screen (88-108) Screen (135-155) Screen (285-305)	November 2003-Present Manual Measurement November 2004-Present Manual Measurement November 2003-Present Manual Measurement

Well ID	Well Name	Well Alias	Land Surface Elevation (ft)	Instrument (Depth from Land Surface) (ft)	Available Data
1804	ICPP-1804	ICPP-1804	4920.96	Screen (246-266) Screen (358-378)	October 2002-Present Manual Measurement December 2002-October 2003 Automated Data October 2002-Present Manual Measurement December 2002-Present Automated Data
1807	ICPP-1807	ICPP-1807	4924.13	Screen (144-164) Screen (230-250) Screen (364-384)	February 2004-Present Manual Measurement February 2004-Present Manual Measurement October 2002-Present Manual Measurement January 2003-October 2003 Automated Data
735	CPP-33-1	33-1	4914.33	Screen (89.0-90.0)	Dry
736	CPP-33-2	33-2	4913.29	Screen (85.8-105.8) Screen (85.8-105.8)	February 1994-May, 2003 Automated Data January 2001-Present Manual Measurement
737	CPP-33-3	33-3	4913.83	Screen (111.8-122.0) Screen (111.8-122.0)	January 1993-October, 1995 Automated Data January 2001-Present Manual Measurement
764	CPP-33-4	33-4	4911.02	Screen (98.2-118.3)	February 1994-April, 2001 Manual Measurement
806	CPP-37-4	37-4	4910.13	Screen (99.6-110) Screen (99.6-110)	February 1992-Present Automated Data January 2001-Present Manual Measurement
131	CPP-55-06	55-06	4911.61	Screen (93.1-113.1) Screen (93.1-113.1)	October 1992-Present Automated Data January 2001-Present Manual Measurement
1057	INTEC-MON-P-001	MW-1-4	4915.85	Screen (326-336) Screen (326-336)	August 2002-Present Automated Data January 2001-Present Manual Measurement
1057	INTEC-MON-P-001	MW-1-1	4915.85	Piezometer (359-369)	Dry
1058	INTEC-MON-P-002	MW-2	4912.3	Screen (102-112) Screen (102-112)	March 1992-Present Automated Data January 2001-Present Manual Measurement
1059	INTEC-MON-P-003	MW-3-2	4915.22	Screen (128-138)	January 2001-Present Manual Measurement
1059	INTEC-MON-P-003	MW-3-1	4915.22	Piezometer (116.3-118)	May 2001-Present Manual Measurement
1060	INTEC-MON-P-004	MW-4-2	4910.63	Screen (100.6-110.6) Screen (100.6-110.6)	February 1994-January, 2001 Automated Data April 2001-March, 2002 Manual Measurement
1060	INTEC-MON-P-004	MW-4-1	4910.63	Piezometer (128.0-129.7)	January 2001-Present Manual Measurement

Well ID	Well Name	Well Alias	Land Surface Elevation (ft)	Instrument (Depth from Land Surface) (ft)	Available Data
1061	INTEC-MON-P-005	MW-5	4915.59	Screen (106.5-126.5) Screen (106.5-126.5)	March 1994-May, 2003 Automated Data May 2001-Present Manual Measurement
1062	INTEC-MON-P-006	MW-6	4915.73	Screen (117-137) Screen (117-137)	February 1994-Present Automated Data January 2001-Present Manual Measurement
1063	INTEC-MON-P-007	MW-7-2	4916.38	Screen (132-142) Screen (132-142)	August 2002-Present Automated Data January 2001-Present Manual Measurement
1063	INTEC-MON-P-007	MW-7-1	4916.38	Piezometer (102.3-104)	Dry
1064	INTEC-MON-P-008	MW-8	4911.72	Screen (115-125)	January 2001-June, 2001 Manual Measurement
1065	INTEC-MON-P-009	MW-9-2	4918.79	Screen (120-130)	January 2001-Present Manual Measurement
1065	INTEC-MON-P-009	MW-9-1	4918.79	Screen (104.2-105.7)	Dry
1066	INTEC-MON-P-010	MW-10-2	4913.88	Screen (141-151) Screen (141-151)	August 2002-Present Automated Data January 2001-Present Manual Measurement
1066	INTEC-MON-P-010	MW-10-1	4913.88	Piezometer (76.5-78)	Dry
1067	INTEC-MON-P-011	MW-11-2	4913.99	Screen (131-136)	January 2001-August, 2001 Manual Measurement
1067	INTEC-MON-P-011	MW-11-1	4913.99	Piezometer (112-113.5)	Dry
1068	INTEC-MON-P-013	MW-12-2	4912.14	Screen (109-119)	January 2001-April, 2001 Manual Measurement
1068	INTEC-MON-P-013	MW-12-1	4912.14	Piezometer (148.6-150.3)	February 2001-April, 2001 Manual Measurement
1069	INTEC-MON-P-014	MW-13	4918.78	Screen (100-105)	Dry
1070	INTEC-MON-P-015	MW-14	4917.23	Screen (94-104)	Dry
1071	INTEC-MON-P-016	MW-15	4917.88	Screen (111.3-131.3)	January 2001-Present Manual Measurement
1072	INTEC-MON-P-017	MW-16	4918.03	Screen (97-107)	Dry
1073	INTEC-MON-P-018	MW-17-2	4918.42	Screen (181.7-191.7)	January 2001-Present Manual Measurement

Well ID	Well Name	Well Alias	Land Surface Elevation (ft)	Instrument (Depth from Land Surface) (ft)	Available Data
1073	INTEC-MON-P-018	MW-17-1	4918.42	Piezometer (263.8-273.8)	Dry
1073	INTEC-MON-P-018	MW-17-4	4918.42	Screen (360-381)	January 2001-Present Manual Measurement
1187	INTEC-MON-P-019	MW-18-2	4913.74	Screen (113.5-123.5)	Dry
1187	INTEC-MON-P-019	MW-18-1	4913.74	Piezometer (394-414)	January 2001-Present Manual Measurement
1074	INTEC-MON-P-020	MW-20-2	4913.08	Screen (133.2-148.4)	January 2001-Present Manual Measurement
1074	INTEC-MON-P-020	MW-20-1	4913.08	Piezometer (96-106) Piezometer (96-106)	August 2002-Present Automated Data April 2003-Present Manual Measurement
1093	INTEC-MON-P-024	MW-24	4906.35	Screen (53.5-73.5)	January 2001-Present Manual Measurement
257	PW-1	PW-1	4917.82	Screen (100-120) Screen (100-120)	August 2002-February, 2003 Automated Data January 2001-March, 2002 Manual Measurement
258	PW-2	PW-2	4916.99	Screen (111-131) Screen (111-131)	August 2002-May, 2003 Automated Data January 2001-December, 2002 Manual Measurement
259	PW-3	PW-3	4916.9	Screen (103-123) Screen (103-123)	August 2002-Present Automated Data January 2001-June, 2002 Manual Measurement
260	PW-4	PW-4	4915.05	Screen (110-150) Screen (110-150)	August 2002-Present Automated Data January 2001-Present Manual Measurement
261	PW-5	PW-5	4916.39	Screen (109-129)	August 2002-May, 2003 Automated Data
262	PW-6	PW-6	4920.61	Screen (105-125)	Dry
499	USGS-50	USGS-50	4913.5	Screen (357-405)	January 2001-Present Manual Measurement

A-3.5 Vadose Zone Water Chemistry

Contaminants have been observed in the INTEC perched water since the 1950s (Robertson et al. 1974), as summarized in the OU 3-13 RI/BRA (DOE-ID 1997). During the spring and summer of 2001, OU 3-13 Group 4 updated the concentration inventory by sampling existing and newly constructed perched water wells for radionuclides and general organic/inorganic chemistry (DOE-ID 2003a). This latter effort also verified the historical chemical analysis from previous investigations. Both data sets were summarized in the Monitoring Well and Tracer Study Report (DOE-ID 2003a). In addition to the Group 4 report, the wells installed during the ICDF construction were sampled for VOCs, SVOCs, metals, and major cations and anions in 2002 (Cahn and Ansley 2004).

The Monitoring Well and Tracer Study Report's (DOE-ID 2003a) analysis of the water chemistry data concluded that the former percolation ponds may impact perched water only as far north as the CS-SP well (DOE-ID 2003a). This conclusion was based on environmental isotopic signatures of the perched water and chloride concentrations in perched water and in the Snake River Plain Aquifer. The Monitoring Well and Tracer Study Report also concluded that the northern perched water in the vicinity of the tank farm receives water from many sources, including leaking pipes, precipitation, the Big Lost River, and possibly the sewage treatment lagoons because of elevated nitrate levels. The nitrate could be from tank farm leaks and spills or the sewage treatment lagoons. However, high radionuclide concentrations in the tank farm vicinity perched water indicate that the tank farm leaks and spills have impacted perched water. The ICDF well data obtained in 2002 suggested that the perched water (shallow, middle, and deep) had the same chemistry as percolation pond water.

These data correspond to the following categories:

- Field parameters (pH, conductivity, dissolved oxygen, temperature, total dissolved solids)
- Hazardous constituents (arsenic, barium, cadmium, chromium, lead, mercury, selenium, silver, fluoride, nitrate, lindane, endrin, methoxychlor, toxaphene, 2,4-D)
- Groundwater quality indicators (calcium, copper, iron, magnesium, manganese, sodium, potassium, chloride, bicarbonate alkalinity, sulfate, phenols, zinc)
- Radionuclides (gross alpha, gross beta, Pu-238, Pu-239/240, Tc-99, Am-241, U-233/234, U-235, U-238, Cs-134, Cs-137, Np-237, I-129, Ra-226, Ra-227, Sr-90, tritium)
- Miscellaneous parameters (Al, Ni, Br, CO₃).

A-3.6 Vadose Zone Water Sources

The perched water bodies at INTEC are a result of low-permeability interbeds, low-permeability basalt flows, and high surface recharge rates. The high INTEC recharge rates are from discharges to the former percolation ponds, natural flows from the Big Lost River, discharges to the sewage treatment lagoons, losses from the facility water distribution system, and infiltration from lawn irrigation and precipitation. Estimates of these discharges were presented in Appendix F of the OU 3-13 RI/BRA (DOE-ID 1997) and are reproduced in Table A-3-7.

To better understand these recharge sources and to identify plant operations responsible for them, a water system engineering study for INTEC was performed in 2003 (DOE-ID 2003b). The engineering study concluded that the INTEC facility uses approximately 1.65 M gal/day (0.344 M kg/day), which was considerably higher than the 0.228 million kg/day recharge rate assumed in Appendix A of the OU 3-13 RI/ BRA (Appendix A, DOE-ID 1997). Due to inherent uncertainty and unreliable data used in the 2003 study, the INTEC process water flow monitoring systems were upgraded in 2004. A separate study of water discharges to the subsurface in the vicinity of the Waste Calcining Facility (WCF) was performed in 2003 (DOE-ID 2004b). The study identified and quantified several facility-related water discharges in the northern INTEC. All of the WCF discharges are included in Table A-3-8.

The Big Lost River is an intermittent stream that flows adjacent to the northwest corner of INTEC. Most of the streamflow infiltrates through the river channel, INL Site spreading areas, or the playas located at the river's terminus, which is located approximately 15 miles north of INTEC. The Big Lost River recharge near INTEC was estimated using stream infiltration losses occurring between the INL Site diversion dam and the Lincoln Boulevard bridge near INTEC. In this river reach, Bennett (1990) estimated the average annual infiltration rate to be 9,800 acre-feet for the period 1965-1987. The distance between the INL Site diversion dam and the Lincoln Boulevard bridge is 10.7 miles, which results in a long-term infiltration rate of approximately 1,900 kg/day per meter of river length.

More recent daily streamflow records obtained from the gauging stations located at the INL Site diversion dam and Lincoln Boulevard bridge (USGS 2004) were used to estimate a transient infiltration rate adjacent to the INTEC. Daily stream -flow data are available from 1984 through the present time. The flow difference between the INL Site diversion dam and Lincoln Boulevard bridge gauges was used to estimate streamflow losses due to infiltration to the river channel along the 10.7-mile river reach. A time series analysis of the data was performed to estimate a lag time between the diversion dam and Lincoln Boulevard gauging station, and the result was a monotonically decreasing correlation with increasing lag. This indicated the water travel time between stations is less than 1 day and simply differencing the daily mean flow at each station for each day provided an adequate estimate of possible infiltration. The average daily infiltration rate for the period 1984-2003 was approximately 1,066 kg/day per meter of river length (Figure A-3-9). As indicated in Figure A-3-9, the river did not flow beyond the INL Site diversion dam during the years 1988 through 1992, 1994, and 2001 through 2003.

Using the changing perched water and soil moisture conditions as model calibration data requires using pre- and post-remedial action discharge rates. The pre-remedial action water sources are summarized in Table A-3-7 and represent the values used in the OU 3-13 RI/BRA. The selected remedy for OU 3-13, Group 4, (perched water) included surface water reduction which resulted in elimination or significant reduction in discharge rates from INTEC facility operations. The former percolation ponds were moved to a new location approximately 2 miles west of INTEC, and several changes were made to INTEC plant operations to reduce recharge sources. The post-remedial action water balance is summarized in Table A-3-8. The post-remedial action water balance, excluding the Big Lost River or precipitation, is 0.242 million kg/day (which is close to the OU 3-13 study value) and reflects the newer data. The differences between water sources in Tables A-3-7 and A-3-8 are due to changes in water use over time at the INTEC and possibly due to more or less conservative estimation methods between the OU 3-13 work and the more recent Group-4 water balance studies.

Some of the water sources provided in Table A-3-7 have been removed since the model was constructed and calibrated. However, they remain in the model because they were performed after model development.

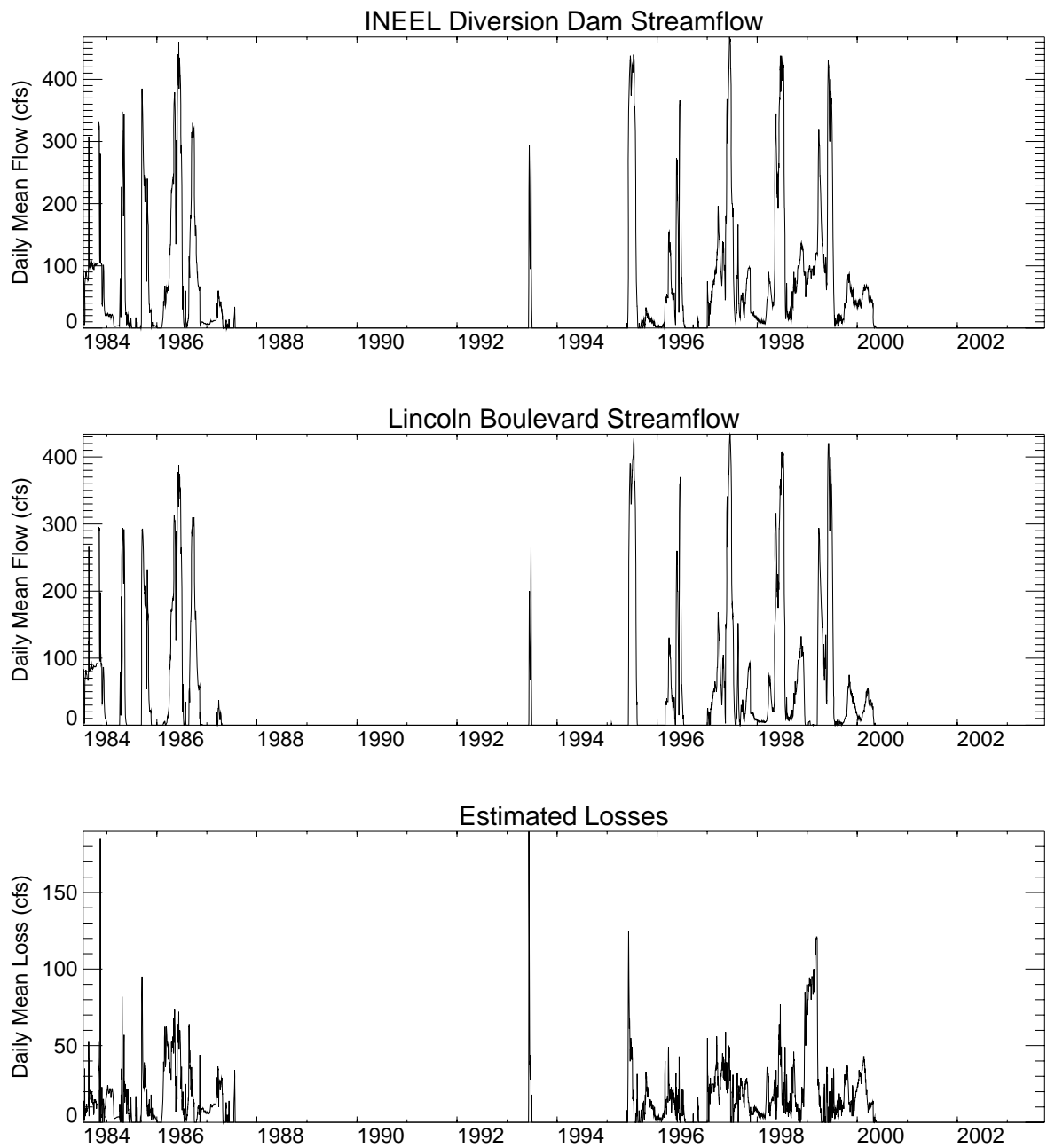


Figure A-3-9. Mean streamflow and Big Lost River losses between the INL Site diversion dam and Lincoln Boulevard bridge.

Table A-3-7. OU 3-13 RI/BRA model water balance (from Tables 1-8 and 1-9 of Appendix F in DOE-ID 1997).

Water Source	Mass Rate (m ³ /day)	Notes
Precipitation Total	462.0	640,000 m ² @18 cm/year and 5,360,000 m ² @1 cm/year
Landscape irrigation total	13.50	—
Steam vent condensate total	17.31	—
Steam Vent Area 1	1.82	—
Steam Vent Area 2	2.29	—
Steam Vent Area 3	1.53	—
Steam Vent Area 4	1.00	—
Steam Vent S-3	3.36	—
Steam Vent S-19	2.09	—
Steam Vent S-76	0.45	—
Steam Vent S-78	0.23	—
Steam Vent S-180	0.78	—
Steam Vent 21	0.42	—
Steam Vent 24	1.62	—
Steam Vent 27	0.22	—
Steam Vent 30	0.67	—
Steam Vent UT-46	0.20	—
Steam Vent UT-47	0.23	—
Steam Vent UT-48	0.39	—
CPP-603 basins	0.51	Estimated from basin makeup water
Sewage treatment ponds	155.56	—
Fire water system leaks total	41.23	Calculated from average fire water system flow estimated prior to 1995
Former percolation ponds	5,838.87	—
Big Lost River	2,100.00	—

Table A-3-8. Current (post-remedial action) water balance from DOE-ID (2003b) and DOE-ID (2004b).

Water Source	Mass Rate (m ³ /day)	Notes
Precipitation total	462.0	640,000 m ² @ 18 cm/year and 5,360,000 m ² @ 1 cm/year.
Landscape irrigation total	13.31	Daily average estimated from 2002 irrigation totals in DOE-ID (2003b). This is higher than the irrigation rates presented in DOE-ID (2004b). Plans to eliminate all irrigation during CY 2006.
Steam vent condensate total	0.30	All but two steam traps have been abandoned or are no longer in use. Rate estimated from RI/BRA for two traps. All have been eliminated.
CPP-603 basins	0	Basin water usage only replaces evaporative losses.
CPP-655 sanitary sewer	0.89	Building 655 septic tank discharge rate (DOE-ID 2004b).
Sewage Treatment Ponds	138.2	Daily average estimated from Nov-01 through Jul-03 totals. Effluent transferred to the vadose zone research park in 2004.
CPP-656 sanitary sewer	4.05	Building 656 septic tank discharge rate (DOE-ID 2004b).
CPP-1606 heating system	0.89	September-April heating steam condensate.
CPP-1608 heating system	0.89	September-April heating steam condensate.
CPP-697 heating system	0.89	September-April heating steam condensate.
Fire water system leaks total	81.77	Calculated from average fire water system flow estimated in 2003.
Steam drip at corner of CPP-649	0.15	—
Steam drip 125ft west of CPP-649	0.15	—
Former percolation ponds	0	Service waste water was transferred to the new location in August, 2002.
Fire hydrant testing	0.13	Fire hydrant testing water is directed towards drainage ditches or use diffusers to maximize evaporation.
Big Lost River	1.90 kg/day/m	Recharge per meter of river length from Bennett (1990).

A-3.7 Vadose Zone Solute Sorption Data

The sorption processes involve mass transfer from the solution to the solids. Sorption is a general term that can be further classified based on the type of process that binds the solute to the solid. These processes include (1) adsorption (solutes held at the mineral surface as a complex), (2) absorption (solutes incorporated into the mineral structure at its surface), and (3) ion exchange (ions sorbed to a surface through changing places with a similarly charged ion on the mineral surface) (Kehow 2001). Contaminant sorption to the subsurface media can significantly slow transport of many contaminants. Simulating sorption requires parameterizing the soil/rock bulk density and adsorption/desorption isotherms for each contaminant. The groundwater model assumes the sorption processes are reversible, and these models lump the processes into a single soil/water distribution coefficient (K_d) parameter. The simulation of the Site CPP-31 Sr-90 transport out of the alluvium did not use the constant K_d parameter approach. The simulation of Site CPP-31 Sr-90 transport used a geochemical model, which considered the important processes that would alter/control the strontium transport from the very high ionic strength of the acidic raffinate. The geochemical conceptual and numerical models are presented in Appendix J.

Reasonably conservative contaminant partition coefficients were identified for each of the COPCs identified in the OU 3-14 RI/FS Work Plan (DOE-ID 2004a) for the three (alluvium, basalt, and interbed)

material types used in the groundwater fate and transport model. Appendix D presents the COPC partition coefficients from site-specific or off-Site transport studies in similar geologic materials. Plutonium is thought to include an immobile and mobile fraction. The total mobile plutonium was estimated to be from 1 to 2.5% (Appendix D) and has a zero K_d . The OU 3-14 COPC and partition coefficients are presented in Table A-3-9. An in-depth discussion of the K_d uncertainty and variability can be found in Appendix D. The minimum Tc-99 K_d value reported in the literature was -0.1 mL/g. The negative value is the result of a column experiment derived K_d value in which the assumed conservative tracer moved slower than the Tc-99. The negative value can not be used to parameterize a contaminant transport model.

Table A-3-9. Preliminary COPCs and partition coefficients.

COPC	Alluvium K_d and (Range) (mL/g)	Interbed K_d and (Range) (mL/g)	Basalt K_d and (Range) (mL/g)
Am-241	400 (100-10,000)	400 (100-10,000)	0.85 (0-140)
C-14	1.6 (0.5-2.8)	1.6 (0.5-2.8)	0 (0-2.8)
Cs-137	50 (10-160)	50 (10-160)	25 (0-44)
Eu-154	400 (15-19,600)	400 (15-19,600)	0.85 (0-140)
H-3	0	0	0
I-129	1.5 (0.04-8.7)	0.7 (0.04-3)	0
Np-237	2 (0.1-60)	2 (0.1-60)	0 (0-8)
Pu-238,239,240 ^a	1,000 (96-12,712)	1,000 (96-12,712)	70 (0-130)
Sr-90	12 (8-20)	50 (25-84)	0.5 (0-15)
Tc-99	0 (-0.1-1.4)	0 (-0.1-0.1)	0
U-234,235,238	1.6 (0.12-12)	1.6 (0.12-12)	0 (0-1.4)
Arsenic	40 (0.7-190)	45 (0.5-230)	2 (0-10)
Chromium	2.4 (0.08-12)	90 (9-673)	1.5 (0-50)
Mercury	118 (118-1,912)	156 (72-673)	0 (0-88)
Nitrate	0.1 (0-0.5)	0.1 (0-0.5)	0
Nitrite	0.1 (0-0.5)	0.1 (0-0.5)	0
a. Pu K_d is for the relatively immobile fraction only.			

A-4 AQUIFER DATA SUMMARY

The Snake River Plain Aquifer is one of the largest and most productive aquifers in the United States, with approximately 9% of the aquifer lying beneath the INL Site. As with the vadose zone, historical investigations by DOE and USGS have provided an extensive set of data describing the aquifer and its hydrogeologic properties. Similar to the vadose zone, the Snake River Plain Aquifer comprises primarily alternating basalt flows and discontinuous interbeds (INEEL 2003b); however, unlike the vadose zone, only one primary sediment unit exists near the INTEC area. Properties specific to the saturated aquifer near INTEC are discussed in the following subsections.

A-4.1 Aquifer Geology/Lithology

For the purposes of contaminant transport predictions, it is necessary to define the top of the water table, the thickness of the aquifer, and the lithology. The depth to the top of the aquifer ranges between 200 ft in the northern and 900 ft in the southern portions of the INL Site, respectively. Under INTEC, the top of the aquifer is located at approximately 450 ft below land surface. Defining the thickness of the SRPA is more difficult, primarily because the thickness of interest for contaminant transport is much less than the total aquifer thickness. The thickness of the aquifer through which water actively flows is uncertain and is based on a limited number of fully penetrating wells (Figure A-4-1). Estimates near the INL Site vary from near zero to over 1,200 ft. To better define this thickness, deep well temperature logs were used by Smith in 2002. The temperature logs reflect an isothermal gradient in the upper portions of the aquifer, with normal temperature gradients occurring deeper. The isothermal region is attributed to cold recharge water moving fast enough to overcome the geothermal gradient. This isothermal area is thought to identify the portion of the aquifer actively conducting water and contaminants.

The lithology was primarily defined by the work by Anderson (1991) who estimated the areal extent of basalt flow groups and sedimentary interbeds in the upper 700 ft of subsurface. In the INTEC and Reactor Technology Complex (RTC), 23 basalt flow groups were identified and designated with informal letters B through I with the I flow being the oldest and deepest. The flow groups included 15 to 20 sedimentary interbeds which were designated by the two alphabetical characters of the basalt flow above and beneath the interbed. Flow group I tends to be many times thicker than other flows near the INL Site, and is overlain by the HI interbed. The HI interbed is widespread, occurs in most wells that penetrate to the flow group I (Anderson 1991), and is the primary sedimentary structure in the INTEC/RTC vicinity.

Data taken from 51 INL Site and USGS well logs were used to define the HI interbed thickness and surface elevation. Data pertaining to older INL Site and USGS wells can be found in Anderson (1989) and Anderson, (1991), and more recent data can be found in DOE-ID (2002). The data available to define the HI interbed thickness and elevation are contained in Table A-4-1. Analysis of this data shows that the HI interbed tends to dip in the southeast direction when viewed from a large scale (OU 3-13 RI/BRA aquifer model domain) and that the interbed tends to become thicker and more continuous in the southeast direction. Isopach maps of the HI interbed can be found in Appendix C. Well logs from Wells SPERT-IV and Site-09 (southeast of INTEC) indicate that the interbed can be approximately 90 ft thick in some areas.

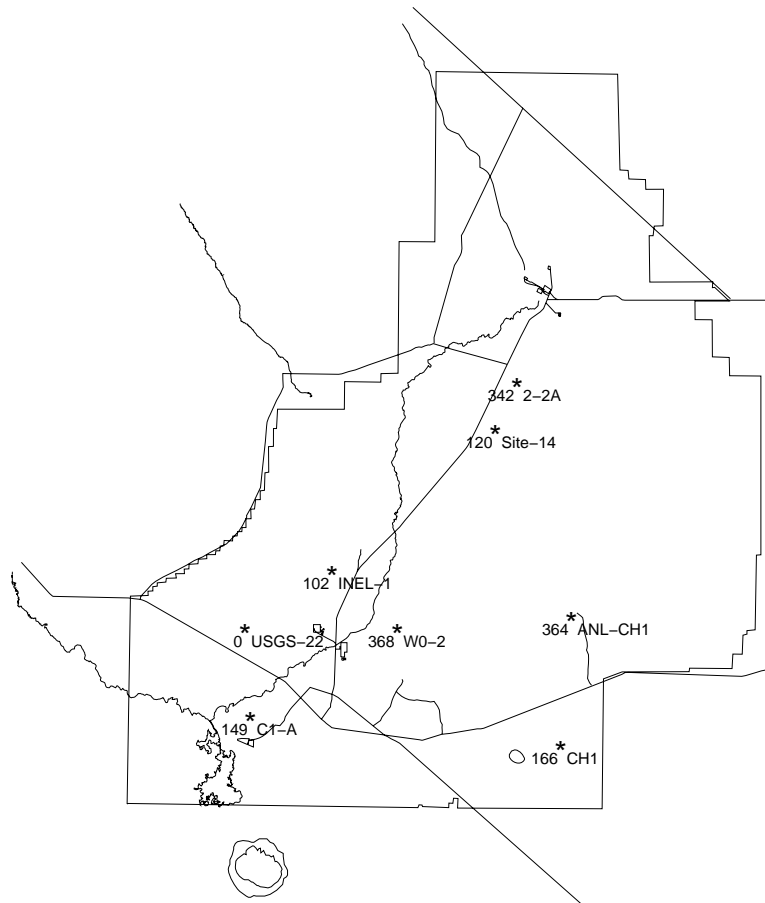


Figure A-4-1. Deep INL Site wells used to define the aquifer thickness (m).

Table A-4-1 HI interbed elevation and thickness data.

Well	Surface Elevation (ft)	Depth to HI Interbed Top (ft)	HI Interbed Thickness (ft)	Well	Surface Elevation (ft)	Depth to HI Interbed Top (ft)	HI Interbed Thickness (ft)
cfa-1	4928.31	623	48	usgs-047	4916.309	532	5
cpp-3	4916.047	519	7	usgs-048	4917.11	549	3
cpp-4	4909.282	523	0	usgs-049	4912.9	540	2
lf2-09	4932.227	625	14 ^a	usgs-051	4918.74	561	4
lf2-10	4932.477	620	49	usgs-052	4909.557	526	5
mtr-test	4917.149	351	0	usgs-057	4922.487	567	5
npr-test	4933.146	556	42	usgs-058	4918.373	342	7

Well	Surface Elevation (ft)	Depth to HI Interbed Top (ft)	HI Interbed Thickness (ft)	Well	Surface Elevation (ft)	Depth to HI Interbed Top (ft)	HI Interbed Thickness (ft)
ow-1	5042.	758	5	usgs-066	4921	365	7
ow-2	5044.	781	6	usgs-067	4914	572	18
rwmc-m04d	5022.53	728	3	usgs-076	4930	528	4
site-09	4926.9	724	84	usgs-079	4931	487	4
site-19	4926.329	462	5	usgs-082	4908	557	9
spert-IV	4924	837	87	usgs-083	4943	716	36 ^a
tra-06a	4926	489	6	usgs-085	4939	631	6 ^a
tra-07	4931	495	6 ^a	usgs-104	4989	688	12 ^a
usgs-020	4916	611	65 ^a	usgs-106	5015	652	0
usgs-034	4929	593	4	usgs-121	4910	517	5
usgs-038	4929	596	5	usgs-123	4920	559	4
usgs-039	4931	568	4	C-1A	5029.	698	5
usgs-040	4916	527	2	EOCR	4943	966	34
usgs-041	4917	530	4	NPR_WO-2	4930	571	27
usgs-042	4918	547	0	S5G-Test	4850	698	26
usgs-043	4916	516	4	WS-INEL-1	4878	670	29
usgs-044	4918	521	0	ICPP-1795	4340	587	7
usgs-045	4920	541	9	ICPP-1796	4331	605	27
usgs-046	4916	542	6	ICPP-1797	4328	601	16
usgs-059	4915	554	4	ICPP-1798	4315	621	57
usgs-065	4925	490	8 ^a				
a. Well did not fully penetrate interbed. CFA=Central Facilities Area. CPP=Chemical Processing Plant (now INTEC). MTR=Materials Test Reactor. RWMC=Radioactive Waste Management Complex. SPERT=Special Power Excursion Reactor Test. TRA=Test Reactor Area (now RTC). USGS=United States Geological Survey.							

A-4.2 Aquifer Hydrological Data

A-4.2.1 Aquifer Hydraulic Conductivity

The results of aquifer well testing can be found in several studies. Ackerman (1991) analyzed 183 aquifer well tests and estimated the transmissivity to range from 1.1 to 760,000 ft²/day. Wood (1989) summarized well pumping tests near the Test Area North and estimated the average transmissivity to be

13,000 ft²/day. Magnuson and Sondrup (1998) reports the aquifer transmissivities in the vicinity of the SDA to be in the range of 1.1 to 1,000,000 ft²/day. ICP (2004) estimated the hydraulic conductivity of Well ICPP-MON-A-230 at the INTEC to be in the range of 2,000 to 4,000 ft/day. Most of the hydraulic data were obtained from single and partially penetrating well tests conducted in the uppermost portion of the aquifer. These transmissivity data were converted to hydraulic conductivity using the well screen thickness, are presented in Table A-4-2, and are thought to be representative of basalt properties.

There are less data available for the HI interbed. Pumping tests have been performed by the State of Idaho (Frederick and Johnson 1996) using packers to isolate the interbed from the surrounding basalt. Geotechnical analysis of interbed samples collected for DOE-ID (2004c) from boreholes ICPP-1795, ICPP-1797, and ICPP-1798 has also provided permeability estimates south of the INTEC. The results of the pumping tests and geotechnical analysis are provided in Table A-4-3.

Table A-4-2 Snake River Plain Aquifer hydraulic conductivity values.

Well Name	Hydraulic Conductivity (ft/day)	Well Name	Hydraulic Conductivity (ft/day)	Well Name	Hydraulic Conductivity (ft/day)
tf-aquifer	2560.	site-19	155.8	usgs-012	104.8
anp-05	1923.1	spert-1	7.1	usgs-014	611.1
anp-06	6666.7	spert-2	299.6	usgs-015	4.5
ara-02	1018.5	tan-01	192.1	usgs-024	200.
arbor-test	5600.	tan-02	160.	usgs-030	5657.9
area-II	754.7	tan-03	182	usgs-031	118.9
cfa-2	1.1	tan-04	49	usgs-037	246.2
cpp-1	973.3	tan-05	335	usgs-040	390.9
cpp-2	2162.2	tan-06	14	usgs-043	355.6
cpp-3	7378.6	tan-07	48	usgs-051	15.8
cpp-4	0.9	tan-08	10	usgs-057	109.8
ebr-I	2.7	tan-09	28	usgs-058	740.
ebr-II-1	5200.	tan-10	502	usgs-076	754.0
ebr-II-2	110.	tan-10a	31	usgs-082	608.7
eocr	967.7	tan-11	16	usgs-083	3.8
fet-disp	156.2	tan-12	3.7	usgs-086	6.5
firesta-2	2000.	tan-13a	14	usgs-087	9.8
hwy-3	3.3	tan-14	0.2	usgs-088	0.2
iet-disp	1.6	tan-15	64	usgs-089	0.9
loft-1	310.	tan-16	122	usgs-090	15.8
loft-2	46.0	tan-18	233.3	usgs-097	582.0
lptf-disp	34.0	tan-19	291.7	usgs-098	826.5
mtr-test	1418.4	tan-19	98.9	usgs-099	1746.0

Well Name	Hydraulic Conductivity (ft/day)	Well Name	Hydraulic Conductivity (ft/day)	Well Name	Hydraulic Conductivity (ft/day)
npr-test	245.7	tan-20	0.9	usgs-100	177.2
nrf-1	3953.5	tan-21	9.6	usgs-101	12.6
nrf-2	4473.7	tan-22a	214.7	usgs-103	8843.0
nrf-3	500.	tan-23	477.2	usgs-104	0.1
omre	1.1	tan-23a	100	usgs-105	634.3
p&w-1	5000.	tan-24	43.5	usgs-106	565.0
p&w-2	2058.8	tan-24a	418.2	usgs-107	327.1
p&w-3	177.2	tan-25	37.5	usgs-108	961.5
pstf	57.3	tan-27	135	usgs-109	604.4
rwmc-m01 s	0.7	tan-28	36.7	usgs-110	51.4
rwmc-m03 s	33.7	tan-29	55.2	usgs-111	0.2
rwmc-m04 d	0.1	tan-30a	35.1	usgs-112	666.7
rwmc-m06 s	1.2	tan-ch1	14.1	usgs-113	1958.8
rwmc-m07 s	33.3	tra-01	7300	usgs-114	0.1
rwmc-m10 s	0.1	tra-03	990.1	usgs-115	0.3
rwmc-prod	226.7	tra-04	1048.2	usgs-116	1.2
rwmc-tw	5512.	tra-disp	151.2	usgs-117	0.2
s5g-test	5797.1	tsf05	0.3	usgs-119	0.01
site-06	18.9	usgs-009	2107.1	usgs-120	2340.4
site-14	368.1	usgs-011	2333.3	ws1-1	1.6

Table A-4-3 Summary of HI interbed permeability values.

Well	Hydraulic Conductivity (ft/day)	Reference
USGS-44	2.28E-01	Fredrick and Johnson (1996)
USGS-45	1.80E-01	Fredrick and Johnson (1996)
USGS-46	1.80E-01	Fredrick and Johnson (1996)

Well	Hydraulic Conductivity (ft/day)	Reference
USGS-59	8.39E-02	Fredrick and Johnson (1996)
ICPP-1795	2.30E-04	DOE-ID (2004c)
ICPP-1795	5.42E-04	DOE-ID (2004c)
ICPP-1797	2.83E+01	DOE-ID (2004c)
ICPP-1797	1.96E+00	DOE-ID (2004c)
ICPP-1798	1.53E-01	DOE-ID (2004c)
ICPP-1798	3.30E+00	DOE-ID (2004c)

A-4.3 Aquifer Water Chemistry

As with the INTEC perched water, contaminants have been observed in the aquifer since the early 1950s. The early aquifer contaminants originated from direct disposal of service waste via the CPP-3 injection well. The radioactive service wastes discharged to the injection well included fission and activation by-products from spent nuclear fuel reprocessing at the INTEC with additional minor contributions from laboratory sink drains.

The PEW evaporator system collected dilute radioactive wastes from a variety of sources and concentrated the dilute waste before sending the concentrate (bottoms) to the tank farm. The PEW vapors were condensed, sampled, and then sent to the service waste. The PEW did not effectively remove the more volatile radionuclides. These volatile radionuclides entering the service waste stream have resulted in large aquifer contamination plumes. To quantify the extent of contamination, DOE and USGS have drilled 68 wells downgradient of the INTEC. Groundwater monitoring data are available from the early 1950s to present in some wells and are presented as part of the aquifer calibration information in Section A-8.

A-5 VADOSE ZONE AND AQUIFER CONCEPTUAL MODELS

This study conceptualizes flow and transport through the vadose zone and aquifer as transient processes in three dimensions. The 3-D model domains are necessary to capture the spatial distribution of the vadose zone and aquifer lithology, water recharge sources, and COC sources. Developing a 1-D model of vadose zone flow and transport would lump most of the vadose zone processes into a simple response function and would require calibrating the 1-D model to large-scale tracer data. Large-scale tracer test data are not available for the INTEC, but there are large amounts of data available that represent different portions of the vadose zone. These data often suggest that water and solute movement is subhorizontal and highly spatially variable. The spatial variability invalidates use of 1-D or 2-D models. On the other hand, a 3-D model may be calibrated to a variety of data and data types, each of which may be available for different areas within the vadose zone. These data include perched water elevations, perched water chemistry, 3-D lithological data, and limited small-scale tracers (i.e., radionuclide and contaminants that only partially penetrate vadose zone).

The vadose zone and aquifer models are time-dependent and use three linked simulation domains. The simulation domains consist of (1) a submodel of the tank farm area alluvium including the fractured basalt down to the 110-ft interbed; (2) the large-scale INTEC vadose zone from north of the Big Lost River to south of the former percolation ponds, including the alluvium, fractured basalt, and interbeds down to the water table; and (3) the aquifer, which extends from approximately the INTEC to the southern INL Site boundary. Flow and transport through the three domains are simulated independently and are linked together with the transient water and contaminant flux from each model feeding the next model domain immediately below. Conceptualization and initial parameterization of the vadose zone models are presented in Section A-5.1. Conceptualization and initial parameterization of the aquifer model are presented in Section A-5.2. The simulation code is discussed in Section A-5.3.

A-5.1 Vadose Zone Model and Parameterization

As described above, the vadose zone model is based on a three-dimensional conceptualization through which transient infiltration and transport occurs. In this model, the following assumptions were made:

- Flow in the fractured basalt is controlled by the fracture network and can be represented by a high-permeability, low-porosity equivalent porous medium.
- Surface water sources are not transient with the exception of the fluxes from the former percolation ponds and recharge from the Big Lost River. Variation in discharge and pumping rates in the other service and potable water wells will be neglected.
- The bottom boundary of the vadose zone model is represented by 101.3 Kpa in the water phase. This corresponds to free drainage at just saturated conditions.
- Lateral boundary conditions are no-flow. This might force water to flow through the vadose zone model near the Big Lost River, and might overly constrain infiltration to remain within the model boundaries, but these boundaries are far from the contaminant sources and should not have an undue negative impact.
- The magnitude of the flux entering through the upper boundary is constrained by field data. Perched water levels and contaminant arrival histories will be used to constrain the in situ distribution of transport velocity through adjustment of permeability and porosity.

Under these assumptions, flow through the vadose zone and within the aquifer can be simulated separately. Transient water and contaminant flux leaving through the lower vadose zone model boundary are first computed using the vadose zone models. The vadose zone model parameters were extracted from the data presented in Section A-3. Details of incorporating the physical data into the numerical framework (model parameterization) are discussed below. Parameterization in order of presentation include hydrogeology/lithology (Section A-5.1.1), spatial extent and discretization (Section A-5.1.2), infiltration (Section A-5.1.3),

and contaminant sources (Section A-5.1.4). The vadose zone model was calibrated to perched water and water quality trends of Tc-99, Sr-90, H-3, and nitrate. The vadose zone model calibration is presented separately in Section A-6.

A-5.1.1 Representation of Lithology

The continuous nature of a numerical model requires interpolation of the sparse observations of hydraulic properties onto a relatively dense simulation grid. As presented in Section A-3, the primary lithology is characterized by fractured basalt that is overlain by alluvium and interspersed with sediment units. Also, as discussed in Section A-3, the moisture content and unsaturated hydraulic characteristics are very much different for basalt than for sediments. These differences - and their magnitudes - present a unique interpolation problem and essentially require that the subsurface lithology be treated as a binary system, with hydraulic properties assigned to the model grid according to the distribution of lithologic type.

As presented in Section A-3.1, the vadose zone lithology is comprised of primary features (alluvium, 110-ft interbed, 140-ft interbed, massive basalt, and 380-ft interbeds); secondary features (miscellaneous sediments); and basalts. The 121 wells in the INTEC facility were used to define the lithology and textural materials in this model. There were six basic phases of this step as listed below:

- 1). Digital elevation models of the surface elevation at INTEC were assigned to the top layer of the model grid.
- 2). Wells within and near the model boundaries were selected. Based on the in-depth lithologic, geologic, and hydrologic characterization summarized in Section A-3.1, textural class and lithologies were assigned over the depth of each well in 1-ft increments. At the end of this step, each foot of elevation in each well had been assigned a textural indicator and a lithology flag. The textural indicator was used in Steps 4 and 5, and the lithology flag determined whether the depth increment belonged to the alluvium, basalt, the 110-ft, 140-ft, Interbed below the massive basalt, or 380-ft interbed, or to the secondary discontinuous sediments.
- 3). The thickness of the alluvium in each well was selected as the first continuous variable to be interpolated. Interbed tops and thicknesses for the 110-ft, 140-ft, Interbed below the massive basalt (BM interbed), and 380-ft interbed constituted the remaining eight continuous variables. Alluvium thickness was available for all but one well. However, not all of the primary sedimentary structures were observed in each well, nor did all wells penetrate each interbed. In wells deep enough to penetrate a given unit, the thickness was assigned a zero if the interbed was not present. Those wells were not used to define the interbed top elevation. After the top and thickness of each unit were defined at all well locations, the data for each unit individually were subjected to a geostatistical analysis to determine spatial correlation structure. The analysis included anisotropic variography, trend surface analysis, and cluster analysis. Results of these analyses for the nine variables are contained in Appendix C and are summarized in Table A-5-1.

Table A-5-1 Geostatistical parameters for the nine continuous variables describing lithology.

Variable	Model	Nugget (unit ²)	Partial Sill (unit ²)	Horizontal Range (m)	Vertical Range (m)
Alluvium Thickness (m)	Spherical	0	10	600	Not Applicable
110-ft Interbed Thickness (m)	Spherical	1	5.5	350	Not Applicable
140-ft Interbed Thickness (m)	Gaussian	0	7	200	Not Applicable
Below Massive Basalt (BM) Interbed Thickness (m)	Spherical	0	11	250	Not Applicable
380-ft Interbed Thickness (m)	Spherical	0	3.7	550	Not Applicable
110-ft Interbed Top Elevation (m amsl)	Spherical	1	5	550	Not Applicable

Variable	Model	Nugget (unit ²)	Partial Sill (unit ²)	Horizontal Range (m)	Vertical Range (m)
140-ft Interbed Top Elevation (m amsl)	Spherical	0	10	400	Not Applicable
Below Massive Basalt (BM) Interbed Top Elevation (m msl)	Spherical	0	40	400	Not Applicable
380-ft Interbed Top Elevation (m msl)	Spherical	0	25	600	Not Applicable

4). Data used in Step 3 were removed from the full set, leaving the lithology and textural information for basalt and discontinuous sediments. Based on textural class, the basalt segments were either assigned either a high or low basalt permeability flag. Also, based on textural category, sediment units were assigned either a high or low sediment permeability flag. The geostatistical correlations for these four categorical variables were then determined using indicator variography for the four permeability categories. The following criteria were used for selecting the lithologic flag:

- High-permeability sediment was assigned to material primarily described as sand or gravel.
- Low-permeability sediment was assigned to any material primarily described as silt, clay, silt-stone, or sandstone.
- High-permeability basalt was assigned to material described as cinders, rubble, void, fractured, scoriaceous, porous, broken, ash, void, top, bottom, or vesicular.
- Low-permeability basalt was assigned to any material described as dense, massive, central, middle, hard, or solid.
- High-permeability sediment or basalt was conservatively assigned to any material if the well log only provided a general basalt or sediment description.
- If no material description was available for a depth interval, it was assumed to be the same as the previous depth interval.

5). The textural information for the each of the primary sedimentary units was also assigned either a high or low permeability class based on the previous criterion, resulting in an additional five categorical variables. These were also subjected to rigorous indicator variography. Results of the indicator variography are presented in Table A-5-2.

Table A-5-2 Geostatistical parameters for the nine categorical variables based on textural class.

Variable	Model	Nugget (unit ²)	Partial Sill (unit ²)	Horizontal Range (m)	Vertical Range (m)
Alluvium Permeability Category NE-SW (E-W)	Spherical	0 (0.01)	0.05 (0.03)	300	Not Applicable
110-ft Interbed Permeability Category	Spherical	0	0.2	100	Not Applicable
140-ft Interbed Permeability Category	Spherical	0	0.2	100	Not Applicable
Below Massive Basalt (BM) Interbed Permeability Category	Spherical	0	0.25	400	Not Applicable
380-ft Interbed Permeability Category	Spherical	0	0.2	300	Not Applicable

Variable	Model	Nugget (unit ²)	Partial Sill (unit ²)	Horizontal Range (m)	Vertical Range (m)
High-Permeability Interbed Sediment not Included in the Four Main Interbeds	Exponential	0.008	0.01	100	30
Low-Permeability Interbed Sediment not Included in the Four Main Interbeds	Exponential	0	0.028	100	30
High-Permeability Basalt	Exponential	0	0.09	80	30
Low-Permeability Basalt	Exponential	0	0.055	80	30

6). Ordinary kriging was used to interpolate the nine continuous variables describing the alluvium and primary sediment interbed tops and thicknesses. Indicator kriging was used to interpolate the nine categorical variables used to determine the permeability within the basalts, primary sedimentary interbeds and secondary sedimentary segments.

The geostatistical approaches used and results of each analysis were based on the rigorous analysis presented in Appendix C. That appendix also presents a discussion of data clustering, trend analysis, and predictive uncertainty. It is worthwhile to mention that the resultant horizontal correlation lengths range from 80 to 600 m which are on the order of the grid block lengths. As a result, the statistical distributions are not exactly reproduced in the model. The resultant distribution of alluvium and subsurface interbed structure is presented in Figure A-5-1 as viewed from the south. The fractured basalt is represented between the colored areas.

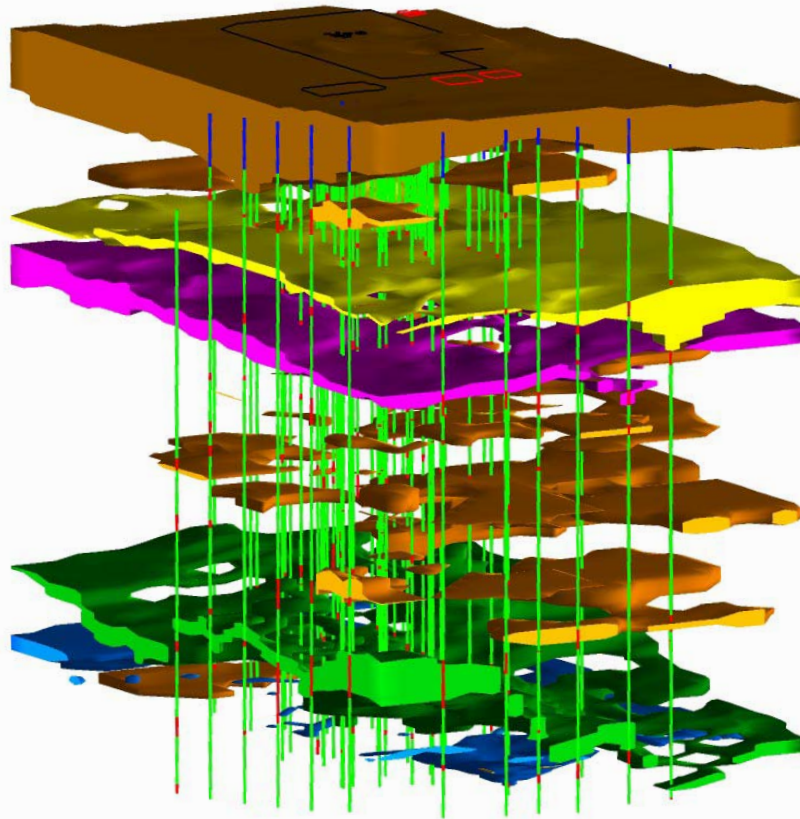


Figure A-5-1. Vadose zone structure. (Surficial alluvium is brown, 110-ft interbed yellow, 140-ft interbed pink, Below Massive Basalt (BM) interbed green, 380-ft interbed blue, and other interbed soils orange. The wells are represented with blue surficial alluvium, green basalt, and red interbed. The INTEC fence, former percolation ponds, and ICDF are outlined on the surface.)

A-5.1.2 Vadose Zone Simulation Domain and Discretization

The vadose modeling used two separate models to predict contaminant fate and transport from land surface to the Snake River Plain Aquifer. The first small-scale model was constructed to represent detailed releases from the tank farm alluvium. It is referred to throughout this document as the “submodel”. The second model is larger in scale and includes the entire INTEC facility from land surface to the Snake River Plain Aquifer. It is referred to as the “large scale, or base-grid model” in the remainder of this document. The contaminant flux leaving the tank farm submodel was placed into the large-scale model immediately below the alluvium/fractured basalt interface. Although the TETRAD simulator has local grid refinement capabilities, it was not used in the vadose zone model to create the tank farm area. A submodel approach was used to improve computational efficiency of the vadose zone models. A linked domain is only necessary if there is feedback between the domains. Drainage out of the alluvium into the fractured basalt below is essentially one-way because the matric potential in the fractured basalt is much less than that in the alluvium.

Selection of the submodel grid was guided by the need to encompass all the OU 3-14 soil sites and maintain grid blocks small enough to accurately simulate the water velocity resulting from the historical liquid releases. This area extended from approximately 100 m northwest of Site CPP-31 to 150 m southeast of Site CPP-31 and used a 20 by 20 grid with 10 m x 10 m grid block sizes. The upper boundary was land surface and the lower boundary was the surface of the 110-ft interbed. The lower boundary was chosen to provide a saturated (perched water) boundary condition, although the contaminant flux from the tank farm submodel was taken at the alluvium/fractured basalt interface. Figure A-5-2 illustrates the submodel's horizontal discretization.

Selection of the large-scale vadose zone model grid was guided by the need to include spatially variable lithology and water recharge sources that may impact contaminant migration from the tank farm near surface to the aquifer. This area includes the Big Lost River to the north and the former location of the percolation ponds to the south. The vadose zone model domain extends in the north-south direction from approximately 300 m north of the northern INTEC fence line to 800 m south of the location of the former percolation ponds. The east-west model domain extends from approximately 200 m west of Lincoln Boulevard to 400 m east of the INTEC steam generating plant. The model's horizontal grid used a 20 by 30 grid with 100 m x 100 m grid block sizes. The model grid was chosen to be large enough to capture major historical and current INTEC recharge sources (i.e., the Big Lost River and former percolation ponds) while being computationally tractable. Large aspect ratios will result in relatively large numerical dispersion which will reduce the required "physical" dispersivity to capture contaminant and water arrival histories.

The vadose zone model's vertical domain extended from land surface to the Snake River Plain Aquifer and used a 1-m vertical discretization in the alluvium and 2-m vertical discretization in the basalt and interbeds. The alluvium discretization was chosen to better define contaminant source depth. Figure A-5-3 illustrates the vadose zone model's horizontal discretization, and Figure A-5-4 illustrates the vadose zone's model vertical discretization. Figure A-5-4 also illustrates the location of the simulated sediment (alluvium and interbed) within the basalt. The white grid blocks are simulated sediment and the red grid blocks are fractured basalt.

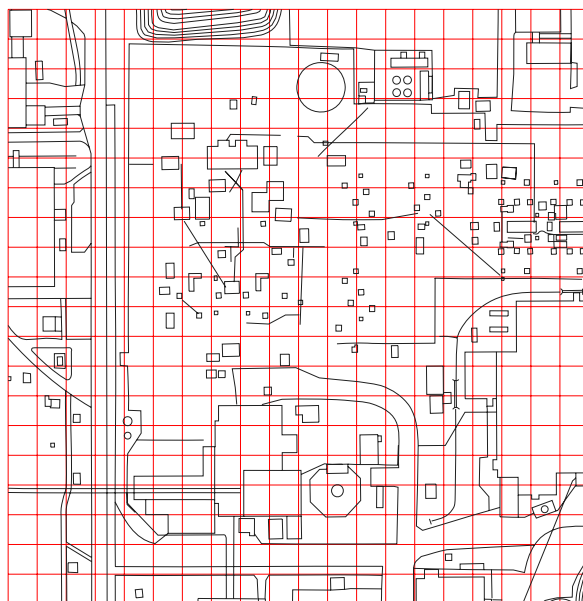


Figure A-5-2. Tank farm submodel vadose horizontal discretization.

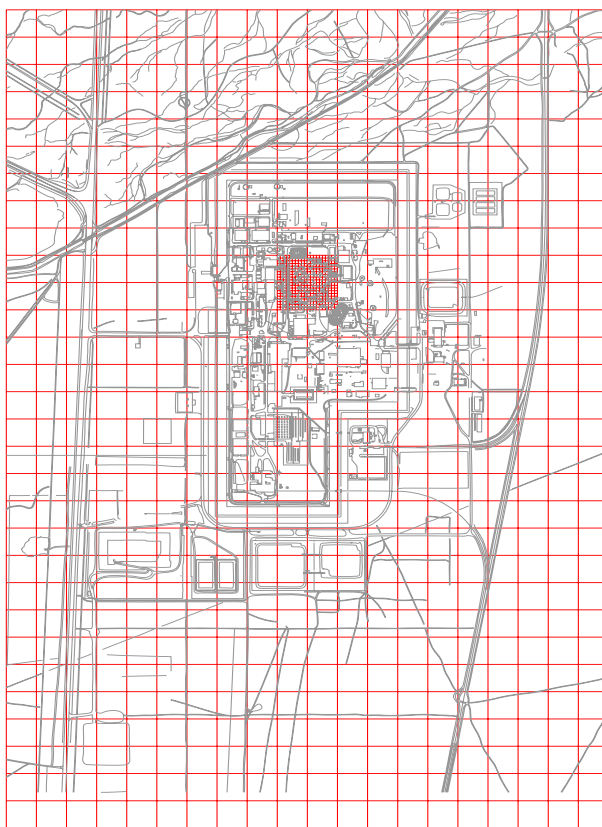


Figure A-5-3. Large-scale vadose zone model horizontal discretization.

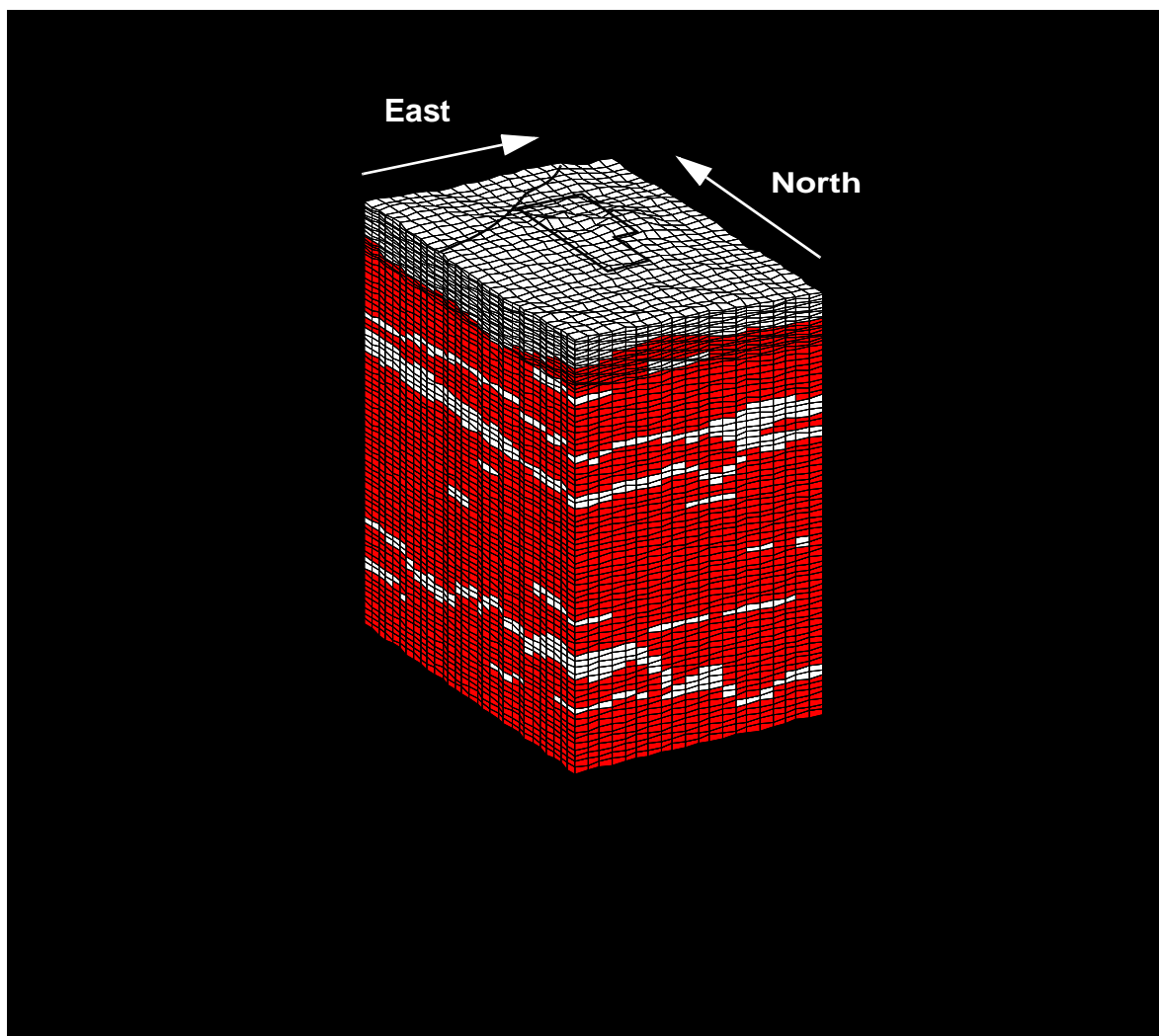


Figure A-5-4. Vadose zone model vertical discretization with 35x vertical exaggeration.

A-5.1.3 Incorporating Infiltration

Infiltration discussed in this section includes recharge from natural and anthropogenic sources. These water sources were presented in Section A-3. For the purposes of simulation, infiltration rate was assumed to be spatially and temporally varying across the INTEC to account for water system leaks, landscape irrigation, sewage effluent, Big Lost River fluxes, etc. In addition, the magnitude of the infiltration rates were time-dependent to account for the reduction in infiltration due to OU 3-13 remedial actions. The pre- and post-remedial action rates identified in Section A-3.6, with some adjustment due to reevaluation of OU 3-13 water sources (Big Lost River and precipitation infiltration), were applied as specified flux to the model surface grid blocks. The pre-remedial action rates represent conditions prior to the percolation pond relocation and implementation of facility-related water recharge controls. The post-remedial action rates represent current conditions. The pre-remedial action infiltration rates were switched to the post-remedial action rates on August 26, 2002. This was the date the percolation ponds were relocated to the vadose zone research park.

The reevaluation of the OU 3-13 water sources included increasing the amount of water from precipitation in the pre-remedial action water balance from 10 cm/year to 18 cm/year to be consistent with the tank farm infiltration study and using a transient Big Lost River infiltration rate from recent USGS streamflow recordings at the INL Site diversion dam and the Lincoln Boulevard bridge (see Section A-3.6). The daily

USGS streamflows (and estimated losses to infiltration) were averaged over 1-year periods when implemented into the model as summarized in Table A-5-3. Figure A-5-5 and Table A-5-4 illustrate the areal distribution and amount of water in the pre-remedial action time periods. Figure A-5-6 and Table A-5-5 illustrate the areal distribution and amount of water in the post-remedial action time period. The area subject to water line leaks was assumed to include the entire developed area at the INTEC, including the steam generation plant located east of the east security fence.

Table A-5-3 Simulated annual average Big Lost River infiltration rate.

Year	Infiltration per Meter of River Length (m ³ /day)
1954-1984	1.9
1985	1.7
1986	3.2
1987	0.8
1988-1992	0.
1993	0.5
1994	0.
1995	1.3
1996	0.9
1997	2.9
1998	2.8
1999	4.2
2000	1.1
2001-2004	0.

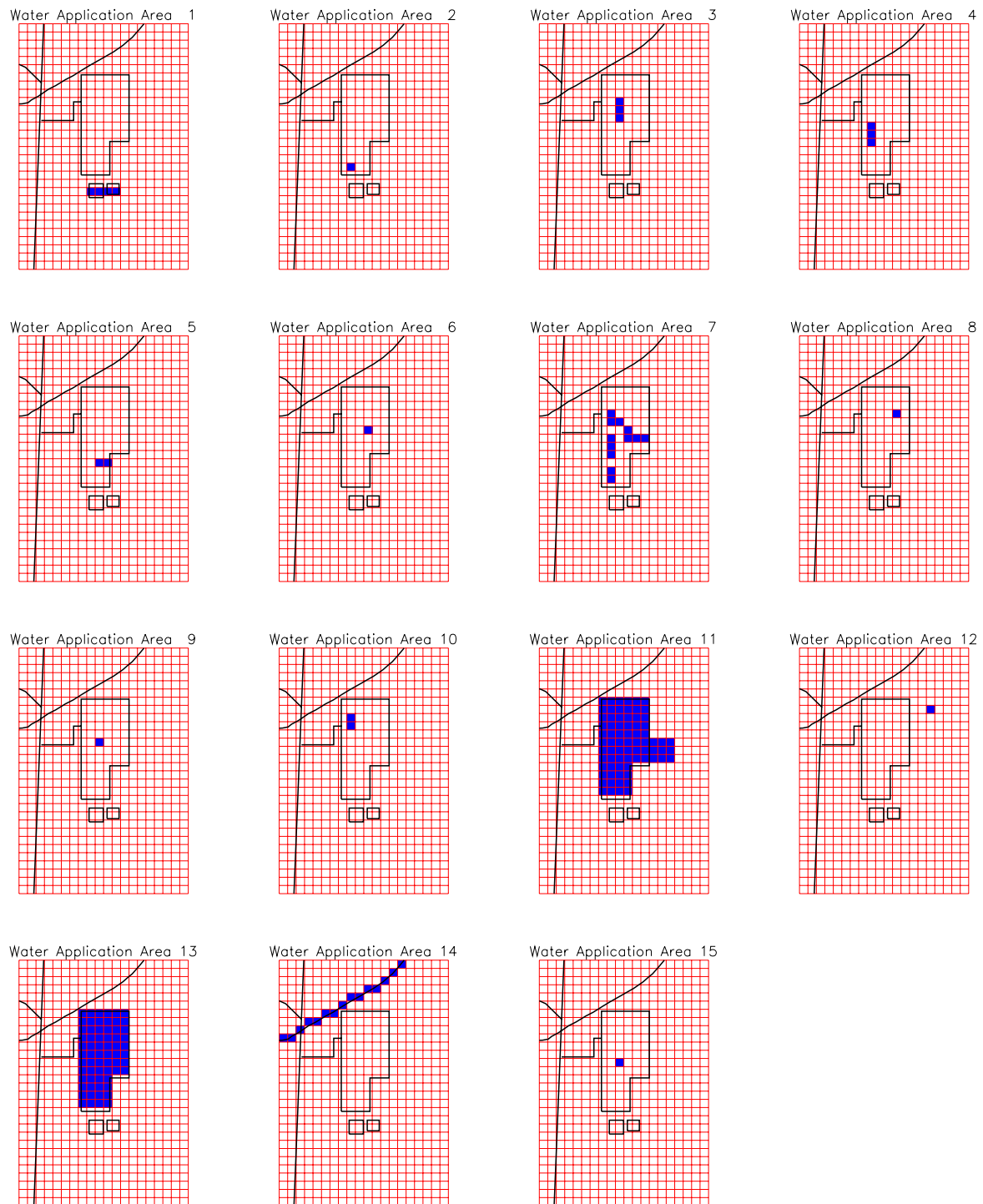


Figure A-5-5. Areal distribution of the pre-remedial action rates.

Table A-5-4 Water application rates for the pre-remedial action corresponding to areas illustrated in Figure A-5-5.

Area Number in Figure A-5-5.	Source Area	Application Rate (kg/day)
1	Percolation ponds	5,838,000
2	Building 603 basins	511
3	Steam vent area	1,821
4	Steam vent area	2,888
5	Steam vent area	1,528
6	Steam vent area	1,002
7	Individual steam vents	10,672. (kg total)
8	Lawn irrigation area	2,245
9	Lawn irrigation area	2,250
10	Lawn irrigation area	8,981
11	Fire water line leaks	41,230
12	Sewage treatment infiltration trench	155,565
13	Developed area precipitation infiltration	315,400
14	Big Lost River	Variable (see Table A-5-3)
15	CPP-3 injection well during failure	Variable (1.321e+10 kg total)

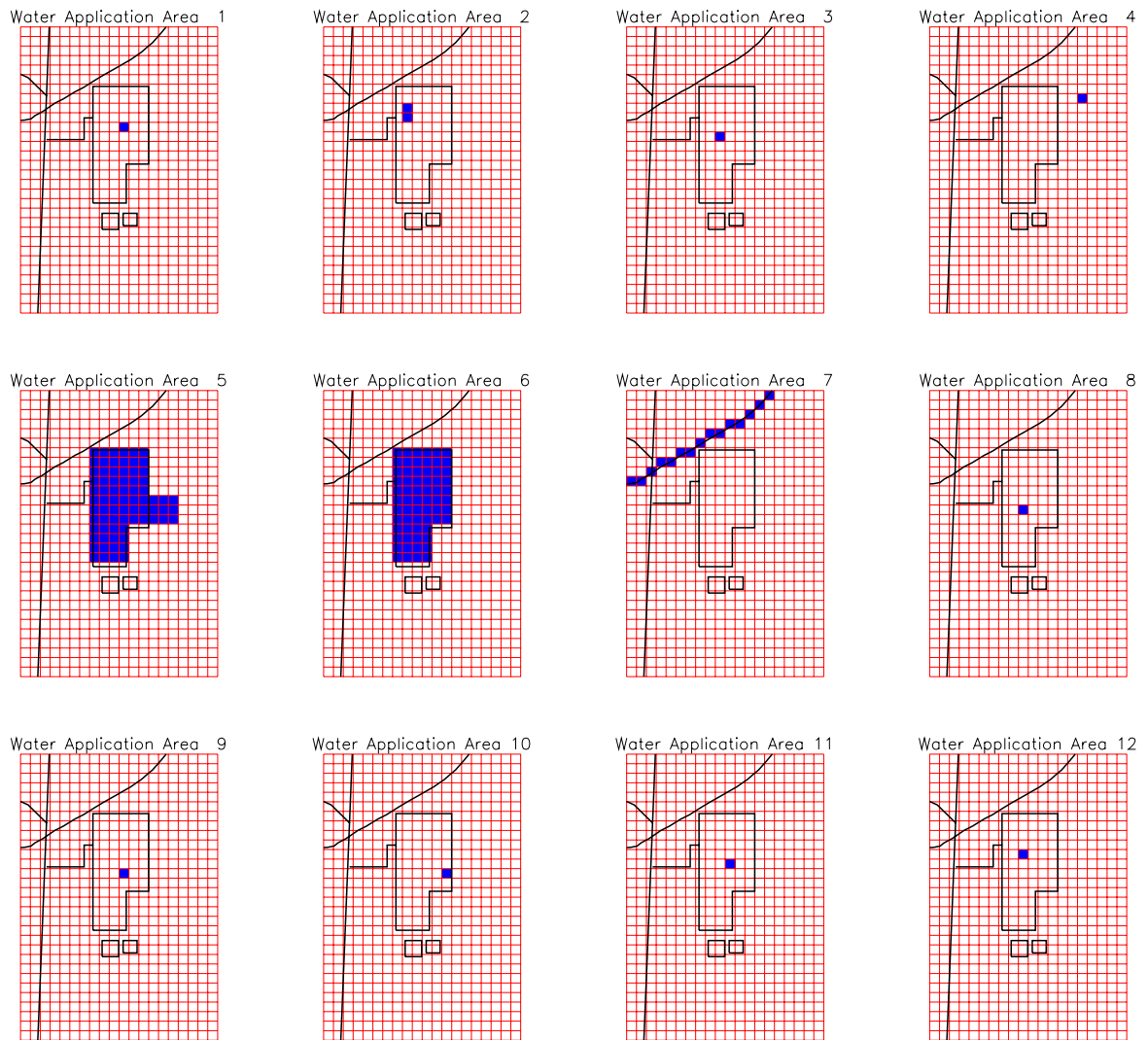


Figure A-5-6. Areal distribution of the post-remedial action water balance.

Table A-5-5 Water application rates for the post-remedial action period corresponding to areas illustrated in Figure A-5-6.

Area Number in Figure A-5-6.	Source Area	Application Rate (kg/day)
1	Steam vent area	303
2	Lawn irrigation	10,646
3	Lawn irrigation	2,661
4	Sewage Treatment Lagoon*	138,181
5	Fire water line leaks with fire hydrant testing	81,901
6	Developed area precipitation infiltration	315,400
7	Big Lost River	Variable (see Table A-5-3)
8	CPP-655 sanitary sewer	890
9	CPP-656 sanitary sewer	4,050
10	CPP-1606 and CPP-697 heating system	1,776
11	CPP-1608 heating system	888
12	CPP-649 steam drip	300
*The sewage treatment effluent was transferred to the vadose zone research park in 2004. However, the model was constructed prior to the transfer and the sewage treatment effluent is included in the simulations.		

A-5.1.4 Contaminant Source Terms for Model Calibration

Parameterizing source terms involved assigning inventories, locations, and times to the known releases. The volume of water and contaminant concentration from each source was quantified and input into the model as a flux rate. The model contaminant source terms were constructed from the data presented in the OU 3-14 RI/BRA, Section A-5, and the OU 3-13 RI/BRA (DOE-ID 1997). The source used in model calibration were the same as those used in the baseline risk assessment and are presented in Section A-8.2.

A-5.1.4.1 Contaminant Source Parameterization

Each of the tank farm and non-tank farm sources are represented in the model as liquid releases placed in specific grid blocks. A complete description of the model source terms is provided in Section A-8.2. The model assumes equilibrium partitioning of sorbing contaminants onto the soil or rock (except Sr-90, see Appendix J). The highly sorbing contaminants will partition into the solid phase after one time step and will behave as a leaching source until sufficient water passes through the source grid block to wash the contaminants deeper into the vadose zone. The source location within the 3-D model domain was the grid block center nearest to the location of the actual leak/spill provided in the OU 3-14 Work Plan (DOE-ID 2004a). Table A-5-6 summarizes each OU 3-14 source location source within the tank farm submodel using a numbering scheme that assigns a unique number to each horizontal model grid block location. Table A-5-7 summarizes each OU 3-13 source location within the large-scale vadose zone model using a similar numbering scheme. The model's horizontal discretization and surface grid block number scheme for source identification is illustrated in Figures A-5-7 and A-5-8 for the tank farm submodel and large-scale vadose zone model, respectively. Grid blocks in the tank farm submodel are 10 x 10 x 1 m. Grid blocks in the upper 18 model layers of the large-scale vadose zone model are 100 x 100 x 1 m, grid blocks in the lower layers are 2 m in the vertical direction.

A-5.1.5 Vadose Zone Initial Conditions

The simulation initial conditions were achieved using the natural recharge sources of 1 cm/year infiltration from precipitation and the long term average Big Lost River infiltration rate (1.9 m/year per meter). The model was run for 1,000 years prior to the transport simulation start time. The 1,000 year initial condition time period was determined by monitoring the maximum grid block pressure change between simulation time steps and extending the initial condition time period until the pressure change is approximately zero.

Table A-5-6 OU 3-14 contaminant source locations and liquid release rate used in tank farm submodel.

Source Identification	Horizontal Grid Block Number	Vertical Layer
CPP-31	250,251,231,232	4
CPP-28	191	3
CPP-79 deep 1967	171	13
CPP-79 deep 1973	171	13
CPP-79 shallow	171	4
CPP-27/33 1964 scrub solution	111,112,131	4
CPP-27/33 1966-1967 scrub solution	111,112,131	4
CPP-27/33 1964-1974 decon solution	111,112,131	4
CPP-15	50	2
CPP-16	228	2
CPP-20	129	2
CPP-24	206,207	2
CPP-25	128	2
CPP-26	258,259,260, 278,279,280, 298,299,300	2
CPP-30	277	2
CPP-32E	257	2
CPP-32W	276	2
CPP-58E 1975 (now CPP-87/89) CPP-58E 1976 (now CPP-87/89) CPP-58W	24,25,26,27,28,29 44,45,46,47,48,49	2

Table A-5-7 Contaminant source locations and liquid release rate used in the large-scale model (OU 3-13 sources).

Source Identification	Horizontal Grid Block Number	Vertical Layer
CPP-89	390	3
CPP-35	371	3
CPP-36/91	391	3
CPP-01/04/05	250	3
CPP-08/09	249	3
CPP-10	250	3
CPP-11	250	3
CPP-03	250,251	3
CPP-17A	271	3
CPP-37A	433	3
CPP-37B	433	3
CPP-14	411	3
CPP-34	474	3
CPP-13	392	3
CPP-06	229	3
CPP-19	289	3
CPP-22	228,229,208	3
CPP-90	370	3
Other Sources		
Service waste injection well (CPP-23)	350 in vadose zone during well collapse	51-61 in vadose zone during well collapse
Early service waste ponds	189,190,191, 192	9
CPP-80	389	3

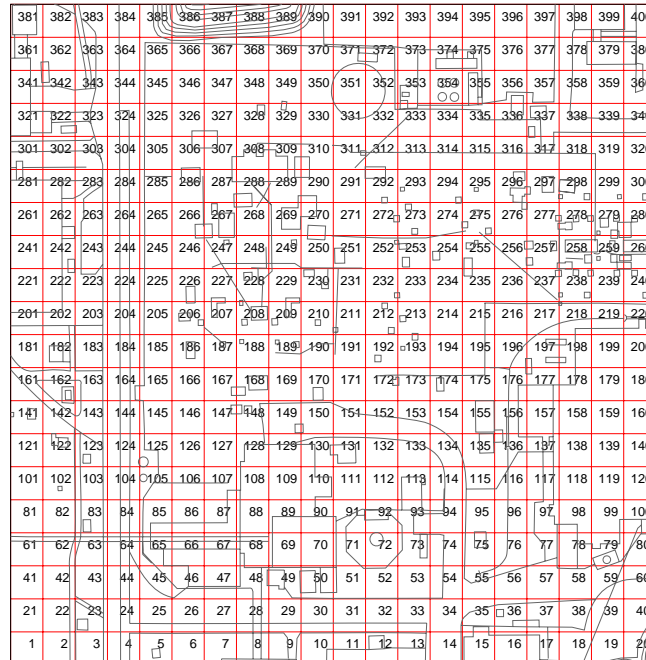


Figure A-5-7. Tank farm submodel horizontal discretization with OU 3-14 source location numbering scheme.

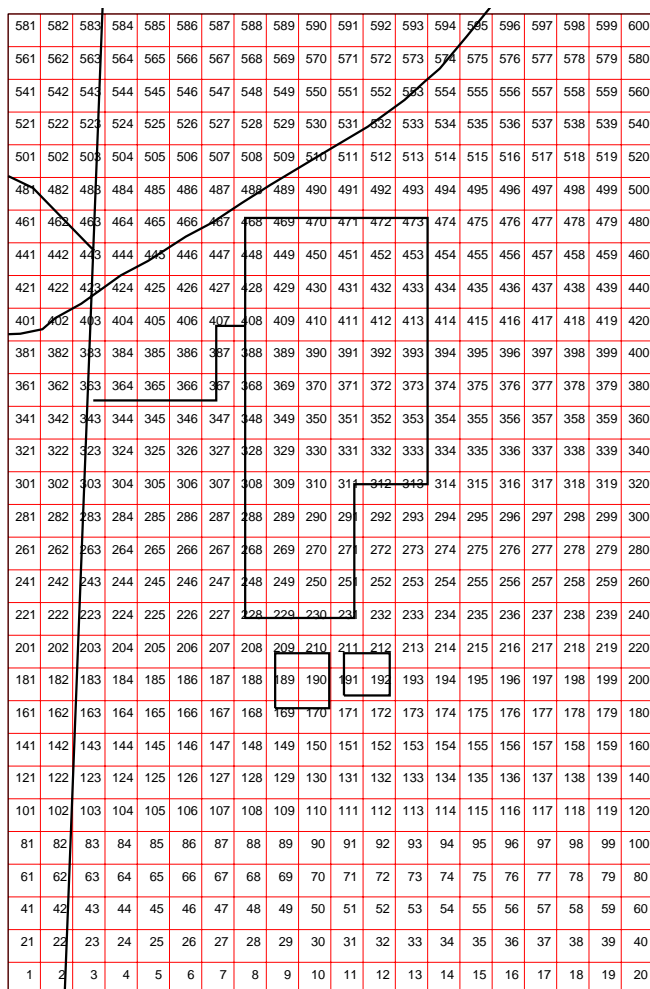


Figure A-5-8. Large-scale vadose zone model horizontal discretization with OU 3-14 source location numbering scheme.

A-5.2 Aquifer Model and Parameterization

The aquifer is parameterized as a three-dimensional flow field with vertical infiltration from the top, a no-flow boundary at the bottom, and lateral Dirichlet boundaries (prescribed head) allowing inflow from the sides. In this model, the following assumptions were made:

- Flow in the fractured basalt is controlled by the fracture network and can be represented by a high-permeability, low-porosity equivalent porous medium.
- The aquifer model domain is assumed to be fully saturated, and the response to pumping and recharge is assumed to behave as if confined. However, a transient water and contaminant flux is placed as an upper boundary condition.

- The top boundary is a vertical flux provided by the vadose zone model near INTEC, the lateral boundary conditions are Dirichlet (prescribed head) allowing inflow from the sides, and the bottom boundary is no flow.
- Isothermal temperature adequately denotes the thickness of the actively flowing portion of the aquifer.
- Water levels measured in the summer of 2004 are representative of the long-term natural gradient.

Details of incorporating the physical data into the aquifer model's numerical framework (model parameterization) are discussed below. Parameterization in order of presentation include hydrogeology/lithology (Section A-5.2.1), spatial extent and discretization (Section A-5.2.2), and boundary conditions and water sources (Section A-5.2.3).

A-5.2.1 Representation of Lithology and Hydrology

The lithology of the aquifer is more uniform than that of the vadose zone. Basalt units tend to be thicker and the sedimentary interbeds are fewer in number. The region extending from north of INTEC to the south of RWMC is primarily comprised of the E through H basalt flows, the HI interbed, and the I basalt flow (Section A-4, and Anderson 1991). In general, the I basalt flow is significantly thicker (Anderson 1991) and may be less permeable than the E through H basalt flows. In the I basalt flow, the high-permeability interflow rubble zones represent a smaller fraction of the total flow thickness. The HI sedimentary interbed separates the overlying higher-permeability basalts from the underlying lower permeability I basalt and may act as a weak confining layer. This separation is captured in the aquifer model through the use of three distinct lithologic types. These include the H basalt, the HI interbed, and the I basalt.

In the model, the H basalt extends downward from the water table and is bounded below by the HI interbed. The I basalt extends from the bottom of the HI interbed to the lower model boundary. The water table elevation was determined by a planar fit to water level data as described above. The top elevation and thickness of the HI interbed was determined in a manner analogous to that used for the primary sedimentary structures in the vadose zone model (i.e., variography and kriging). Elevation of the lower model boundary was based on the thickness of the actively flowing portion of the aquifer (Section A-4.1). These features are illustrated in Figures A-5-11 and Figure A-5-9.

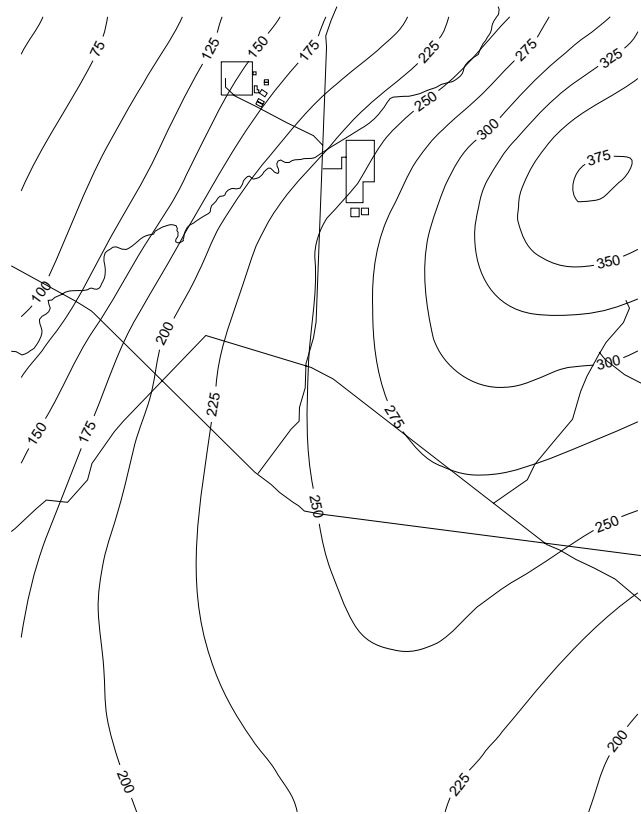


Figure A-5-9. Aquifer model thickness (m).

Nested variograms were used to describe the HI interbed thickness and top elevation (Table A-5-9). Both parameters exhibited smooth variation at short correlation and larger variance at longer lag distances. Kriging the HI interbed resulted in a thick region through the east-central areas of the model grid, with the thick regions extending further south than north. Most of the HI interbed in the west was very thin, and, in the north-central regions, the HI interbed had zero thickness. The krigged top elevation was low in the east, had a ridge running from the center of the southern border to the northeast corner, and was mostly level with a bump in the center North boundary. The low elevation areas in the south correspond to the thick interbed areas. The interpolated thickness and elevation both conformed quite well to observed values where data were available. However, in the northwest and southeast corners, large areas were without data. Uncertainty in the krigged results is high in those areas as reflected by high kriging variance (Appendix C).

Variography was used to determine the geostatistical parameters describing aquifer pump test-derived permeability within the H and upper I basalt units. The variogram for aquifer permeability was modeled with a one-structure variogram, although two structures may have been present. Both variograms were used to predict natural log of permeability onto the grid with almost identical results. Parameters for the simpler one-structure model were used for this work, and the parameters are given in Table A-5-8. Natural log permeability was then interpolated onto the model grid using ordinary kriging. Actual permeability was obtained through back-transformation. A complete description of the variogram structures and ranges used in predicting the aquifer's H basalt permeability field can be found in Appendix C.

Initial permeability values for the current model's HI interbed were estimated from perched water slug tests and core analysis of the HI interbed. Initial permeability values for the current model's I basalt were taken from the OU 3-13 RI/BRA. Figure A-5-10 illustrates the initial H basalt hydraulic conductivity.

Table A-5-8 Geostatistical parameters for the HI interbed thickness and elevation.

Variable	Model	Nugget (Unit ²)	Partial Sill (Unit ²)	Horizontal Range (m)	Vertical Range (m)
HI interbed thickness (range less than 2,300 m)	Gaussian	0.	10	2,300	Not Applicable
HI interbed thickness (range greater than 2,300 m)	Spherical	0.	55 (45 plus the sill of 10 from the first structure)	4,500	Not Applicable
HI interbed elevation (range less than 2,300 m)	Gaussian	0.	340	2,000	Not Applicable
HI interbed elevation (range less than 2,000 m)	Spherical	0.	800 (460 plus the sill of 340 from the first structure)	3,500	Not Applicable
HI interbed elevation (range greater than 2,000 m)	Spherical	0.	1700 (900 plus the sill of 800 from the second structure)	6,000	Not Applicable
H and I basalt permeability (natural log K)	Spherical	2	9	4,000	Not Applicable